frontiers | Frontiers in Immunology

TYPE Original Research
PUBLISHED 27 September 2022
DOI 10.3389/fimmu.2022.910705

OPEN ACCESS

EDITED BY
Christophe Caux,
INSERM U1052 Centre de Recherche en Cancerologie de Lyon, France

REVIEWED BY
Julie Helft,
INSERM U932 Immunité et Cancer, France
Sreekumar Balan,
Icahn School of Medicine at Mount Sinai, United States

*CORRESPONDENCE
Sunil Kumar Raghav
sunilraghav@ils.res.in;
raghuvanshi2010@yahoo.co.in

†These authors have contributed equally to this work

SPECIALTY SECTION
This article was submitted to Antigen Presenting Cell Biology, a section of the journal Frontiers in Immunology

RECEIVED 01 April 2022
ACCEPTED 25 August 2022
PUBLISHED 27 September 2022

CITATION
Jha A, Ahad A, Mishra GP, Sen K, Smita S, Minz AP, Biswas VK, Tripathy A, Senapati SB, Gupta B, Acha-Orbea H and Raghav SK (2022) SMRT and NCoR1 fine-tune inflammatory versus tolerogenic balance in dendritic cells by differentially regulating STAT3 signaling.
Front. Immunol. 13:910705.
doi: 10.3389/fimmu.2022.910705

SMRT and NCoR1 fine-tune inflammatory versus tolerogenic balance in dendritic cells by differentially regulating STAT3 signaling

Atimukta Jha[1,2†], Abdul Ahad[1,2†], Gyan Prakash Mishra[1,3†], Kaushik Sen[4], Shuchi Smita[1,2], Aliva Prity Minz[1], Viplov Kumar Biswas[1,3], Archana Tripathy[3], Shantibhushan Senapati[1,2], Bhawna Gupta[3], Hans Acha-Orbea[5] and Sunil Kumar Raghav[1,2*]

[1]Immuno-genomics & Systems Biology laboratory, Institute of Life Sciences (ILS), Bhubaneswar, OR, India, [2]Manipal Academy of Higher Education, Manipal, KA, India, [3]Department of Biotechnology, Kalinga Institute of Industrial Technology (KIIT), Bhubaneswar, India, [4]Regional Centre for Biotechnology, NCR Biotech Science Cluster, Haryana, India, [5]Department of Biochemistry Center of Immunity and Infection Lausanne (CIIL), University of Lausanne (UNIL), Epalinges, Switzerland

Dendritic cell (DC) fine-tunes inflammatory versus tolerogenic responses to protect from immune-pathology. However, the role of co-regulators in maintaining this balance is unexplored. NCoR1-mediated repression of DC immune-tolerance has been recently reported. Here we found that depletion of NCoR1 paralog SMRT (NCoR2) enhanced cDC1 activation and expression of IL-6, IL-12 and IL-23 while concomitantly decreasing IL-10 expression/secretion. Consequently, co-cultured $CD4^+$ and $CD8^+$ T-cells depicted enhanced Th1/Th17 frequency and cytotoxicity, respectively. Comparative genomic and transcriptomic analysis demonstrated differential regulation of IL-10 by SMRT and NCoR1. SMRT depletion represses mTOR-STAT3-IL10 signaling in cDC1 by down-regulating NR4A1. Besides, *Nfkbia* and *Socs3* were down-regulated in *Ncor2* (*Smrt*) depleted cDC1, supporting increased production of inflammatory cytokines. Moreover, studies in mice showed, adoptive transfer of SMRT depleted cDC1 in OVA-DTH induced footpad inflammation led to increased Th1/Th17 and reduced tumor burden after B16 melanoma injection by enhancing oncolytic $CD8^+$ T-cell frequency, respectively. We also depicted decreased *Ncor2* expression in Rheumatoid Arthritis, a Th1/Th17 disease.

KEYWORDS

SMRT and NCoR1, dendritic cells, Th1/Th17 T-cell response, mTOR-STAT3-IL10 signaling, Nr4a1, comparative genomic and transcriptomic (RNA-seq and ChIP-seq)

10.3389/fimmu.2022.910705

Introduction

Dendritic cells (DCs) play an important role in immune surveillance and maintain an optimal balance between inflammation and immune-tolerance to avoid immune-pathology (1, 2). After encountering pathogens DCs undergo activation and maturation leading to secretion of cytokines and expression of co-stimulatory molecules, which ultimately decides the fate of a particular T-cell response to clear the invading pathogens (3). Hence, antigen specific activation of DCs is an important event to orchestrate the immune system culminating into development of T-cell adaptive response for the induction and expansion of either an optimum protective pro-inflammatory or tolerogenic response (4). DC subtype specific differential expression of toll like receptors (TLRs) along with their unique signaling cascades provide the specificity against the pathogens e.g., plasmacytoid DCs (pDCs) highly express TLR7 and TLR9, required to mount antiviral response whereas conventional DCs (cDCs) are mainly responsible to maintain the balance between inflammatory *vs.* tolerogenic response and cross presentation (5–7). Among cDCs, cDC1 ($CD8\alpha^+$ DCs) are considered as bystanders which integrate signals derived from intracellular infection to tailor the appropriate $CD4^+$ T-cell response along with anti-tumor $CD8^+$ T-cell activation with the help of their unique property of cross presentation (8). cDC1 identify pathogen associated molecular patterns (PAMPS), such as bacterial un-methylated CpG-DNA or viral double stranded RNA through TLR9 and TLR3 respectively (9). Upon TLR9 stimulation in cDC1, the TIR domain of TLR and an adapter, Myd88, activates interleukin-1 receptor-associated kinase-4 (IRAK4) and IRAK1 (10). IRAK4 subsequently activates the NF-kB signaling (11). The TLR9-Myd88 signaling has also been linked with JAK-STAT signaling pathway for cytokines production (12). STAT3 is a new entry in the block although the TLR-Myd88-STAT3 signaling does not affect NF-kB signaling in B-cells (13). STAT3 depleted DCs have been shown to be insensitive to IL-10 mediated suppression leading to hyper-activation of T-cells and inflammation in mice (14). A combination of such divergent DC signals leads to differentiation of naive T helper cells to various effector subtypes such as Th1, Th2, Th17 or Tregs. A fine balance of secretory cytokines like IL-6, IL-12, and IL-23 modulates Th cells towards Th1 or Th17 subtypes, whereas increased levels of IL-10, SOCS3 and CD83 differentiate them towards Tregs (15). Thus, a tight regulation of these cytokines is important to maintain the fine balance between inflammatory, anti-inflammatory or tolerogenic responses (16). The idea of perturbing T-cell differentiation to modulate the immune system for cell mediated therapy is an accepted concept. For example, the use of DCs to manipulate T-cells in cancer immunotherapy has been widely reported. Despite a number of attempts, there are multiple occurrences of insufficient T-cell activation and effective priming in *in vivo* systems (8). Therefore, identifying ways to perturb DC responses in a controlled manner to enhance T-cell function is an interesting area. Recently, NF-kB signaling was shown to be perturbed in tolerogenic DCs having increased IL-10 production (17). However, the regulators underlying the fine modulation of these TFs are not clearly documented. A group of TFs belonging to nuclear receptors (NRs) such as NR4A1 (NUR77) and PPAR-γ are reported to have a role in regulation of cytokine gene expression (18). NURR-77 controls production of IL-6, TNF-α, and IL-12 in both human and murine dendritic cells (19). Similarly, peroxisome proliferator-activated receptor (PPAR-γ) also exerts anti-inflammatory effects in monocytes and macrophages (20). Although TFs and NRs lead to activation of transcription, their activity is tightly regulated by a network of co-regulators, including co-activators and co-repressors. For example, co-regulators ASC-2 and SMRT control activation and repression of Nur77 respectively (21). While ASC-2 is dependent on CaMKIV for the transactivation of Nur77, SMRT on the contrary binds directly to Nur77, through its C-terminal domain nuclear receptor interaction motif and represses it (21). All these observations are made in HeLa and CV-1 cells. Nuclear receptor co-repressor 1 (NCoR1) and its paralog Silencing mediator of retinoic acid and thyroid hormone receptor (SMRT) were identified in relation to unliganded thyroid and retinoic acid receptor mediated repression of gene expression (22). *Ghisletti et al.* has shown that the combination of NCoR1 and SMRT is required for regulation of inflammatory and anti-inflammatory genes in macrophages (23). Recent report showed that siRNA mediated depletion of SMRT in IL4 and GM-CSF differentiated DCs led to decreased expression of CD209 mRNA (24). However, the combinatorial role of NCoR1 and SMRT in immune response regulation in DCs is largely unexplored. Recently we demonstrated that active repression of tolerogenic genes like IL-10 by NCoR1 is essential for development of immunogenic response in DCs (25). NCoR1 depletion enhanced the expression of tolerogenic molecules like IL-10, IL-27, PDL1 and SOCS3 resulting in increased frequency of Tregs and shift of immunogenic balance towards tolerance (25).

In this study, we explored the role of SMRT in modulating the immune function of cDC1 DCs *in vitro, ex vivo* and *in vivo*. We identified how two highly homologous nuclear receptor co-repressor proteins NCoR1 and SMRT tightly control the fine balance of inflammatory and tolerogenic response in DCs, which consequently regulates the differentiation of naïve Th cells into Th1, Th17 or Tregs. Moreover, comparative genome-wide binding of NCoR1 and SMRT and transcriptomic analysis of NCoR1 and SMRT depleted cDC1 revealed their differential role in control of STAT3 signaling and IL-10 expression and its underlying control of repression. Overall, our study demonstrated that NCoR1 and SMRT are potential targets for

regulating a fine balance of DC mediated inflammatory and tolerogenic T-cell responses.

Results

SMRT KD cDC1 DCs depicted enhanced activation/co-stimulation

To identify the potential role of SMRT in cDC1 we first checked the expression of Nuclear Receptor Co-repressor-2 (*Ncor2*) at transcript level in murine cDC1 (mutu-cDC1 line) and observed constitutive expression before and after 2h, 6h and 12h of activation by TLR9 ligand, CpG-B (26) (Supplementary Figure 1A). Next, we generated stable *Ncor2* gene knock down (SMRT KD) and empty vector transduced (control) cDC1 mutu-cDC1 lines. *Ncor2* gene depletion was confirmed at transcript (>75-80%) and protein level in unstimulated and 6h CpG challenged conditions (Figure 1A and Supplementary Figure 1B). Then, we performed RT-qPCR to check mRNA expression of pro-inflammatory (*Il12b*) and anti-inflammatory (*Il10*) cytokine in control and SMRT KD cDC1 cells before and after 2h and 6h CpG challenge. We found significantly increased *Il12b* with a concomitantly decreased *Il10* expression post CpG stimulation in SMRT KD cDC1 compared to control cells (Figure 1A). Besides, flow cytometric analysis showed significantly increased percent positive cells and for co-stimulatory molecules (CD80, CD86 and CD40) in SMRT KD cDC1 as compared to controls (Figure 1B and Supplementary Figure 1C). We observed a similar increase in expression of co-stimulatory molecules in TLR3 activation condition using poly I:C (Supplementary Figure 1D). Next, we investigated the antigen presentation ability through expression of MHC-II and MHC-I in SMRT depleted DCs. We found significantly increased MHC-I percent positive cells in both CpG and pIC activation whereas MHC-II levels remained unchanged (Figure 1B and Supplementary Figure 1D). The MFI shifts for MHC-II and MHC-I molecules also depicted similar trends. Uniform gating strategies were used for analysis of all the costimulatory and antigen presentation markers in the MutuDC cell line. First gate was set on forward scatter- area (FSC-A) and FITC since the cell line has a GFP reporter, then doublets were excluded by gating side scatter SSC-A and SSC-H (Supplementary Figure 1E). To further validate the impact of SMRT depletion *ex-vivo*, we performed transient depletion of SMRT in bone-marrow derived cDC1 (BMcDC1) cultured using FLT3L. First, we confirmed *Ncor2* depletion in BMcDC1 by RT-qPCR and we observed 40% knock down compared to control (Supplementary Figure 2A). Then, we checked the expression of CD80, CD86 and MHC-II using flow cytometry after 18h CpG stimulation and observed significant increase in SMRT KD BMcDC1 compared to controls whereas MHC-I showed an increasing trend (Figure 1C and Supplementary Figure 2C). Uniform gating strategies were used for analysis of BMcDC1 (See methods for details) (Supplementary Figure 2B).

SMRT depleted cDC1 showed increased IL-6, IL-12 and IL-23 pro-inflammatory cytokines with concomitantly decreased IL-10

Next, we checked the expression of important DC response cytokines in both, cDC1 line (mutuDC) and the primary BMcDC1. We found that SMRT depletion significantly enhanced the percent positive cells as well as MFI shifts for IL-6, IL-12p40 and IL-23p19 cytokines after 6h CpG and pIC challenge as compared to control cDC1 line (Figure 2A and Supplementary Figures 3A, B). IL-23p19 was significantly increased in SMRT KD cDC1 in both unstimulated and 6h CpG activated cDC1. On the contrary, IL-10 was significantly reduced upon CpG and pIC activated SMRT KD cDC1 line compared to control (Figure 2A and Supplementary Figures 3A, B). Uniform gating strategies were used for all intra cellular staining throughout cDC1 analysis (Supplementary Figure 3C). Further to estimate the levels of these cytokines in CpG activated cDC1 line in culture supernatants, we performed bio-plex assays and found that the secretory levels of IL-6, IL-12p40 and IL-12p70 were significantly increased in SMRT depleted cDC1 line along with concomitant decrease in IL-10 (Figure 2B). Moreover, IL-2, an important cytokine for T-cell clonal expansion, was also found to be significantly increased in SMRT KD cDC1 compared to controls (Supplementary Figure 4A). We further extended these findings in 18h CpG stimulated primary BMcDC1. Similar to our DC line, we observed a significant increase in percent positive cells and an increasing trend in MFI of IL-6 and IL-23 whereas IL-10 showed reduced expression in SMRT KD BMcDC1 compared to control. However, IL-12p40 percent positive cells and its MFI in SMRT KD BMcDC1 were although higher but not significant compared to control (Figure 2C and Supplementary Figure 4B). We performed bio-plex to quantify cytokines in control and SMRT KD BMcDC1 activated for 6h with CpG. The cytokines secreted by BMcDC1 were not as robust as cDC1 line (Supplementary Figure 4C). These observations suggested a strong inflammatory phenotype for SMRT KD cDC1.

Co-culture of OT-II $CD4^+$ Th cells with SMRT depleted cDC1 enhanced Th1 and Th17 differentiation

To understand the functional impact of SMRT depleted cDC1 response on $CD4^+$ Th cell proliferation and differentiation, we performed a co-culture experiment of purified $CD4^+$ T-cells isolated from spleen of OT-II transgenic

10.3389/fimmu.2022.910705

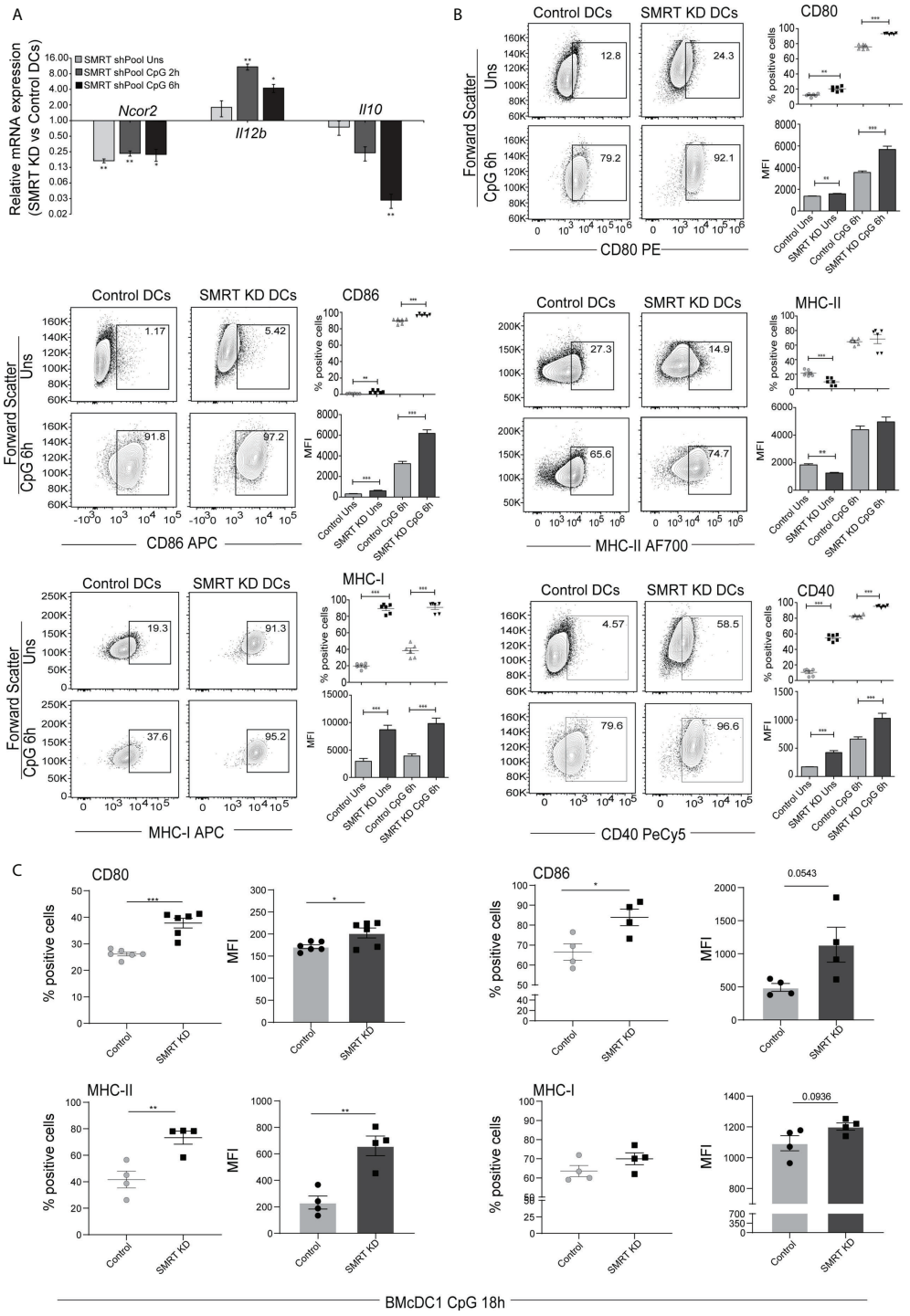

FIGURE 1
SMRT depleted cDC1 and BMcDC1 exhibit enhanced activation and maturation upon TLR9 ligation with CpG-B **(A)** RT-qPCR showing relative transcript expression of *Ncor2*, *Il12b* and *Il10* in unstimulated, 2h and 6h CpG-B stimulated SMRT KD cDC1 (n=3). **(B)** Flow cytometry analysis of co-stimulatory surface markers CD80, CD86, MHC-II, MHC-I, and CD40 in unstimulated and 6h CpG stimulated control and SMRT KD cDC1 line. Corresponding contour plots, dot plots, and bar-plot showed the percent positive cells and MFI shifts for each of the marker genes (n=6). **(C)** Scatter plot and scatter dot plot with bar depicting percent positive cells and MFI respectively of CD80, CD86, MHC-II and MHC-I in 18h CpG stimulated control and SMRT KD bone-marrow derived cDC1 (BMcDC1) (n=4-6). *p ≤ 0.05, **p ≤ 0.01 and ***p ≤0.001. p-value has been calculated using two tailed paired **(A, B)** and unpaired **(C)** student's t-test. Data shown in figure is combined from three independent experiments **(A–C)**. Error bars represent SEM.

10.3389/fimmu.2022.910705

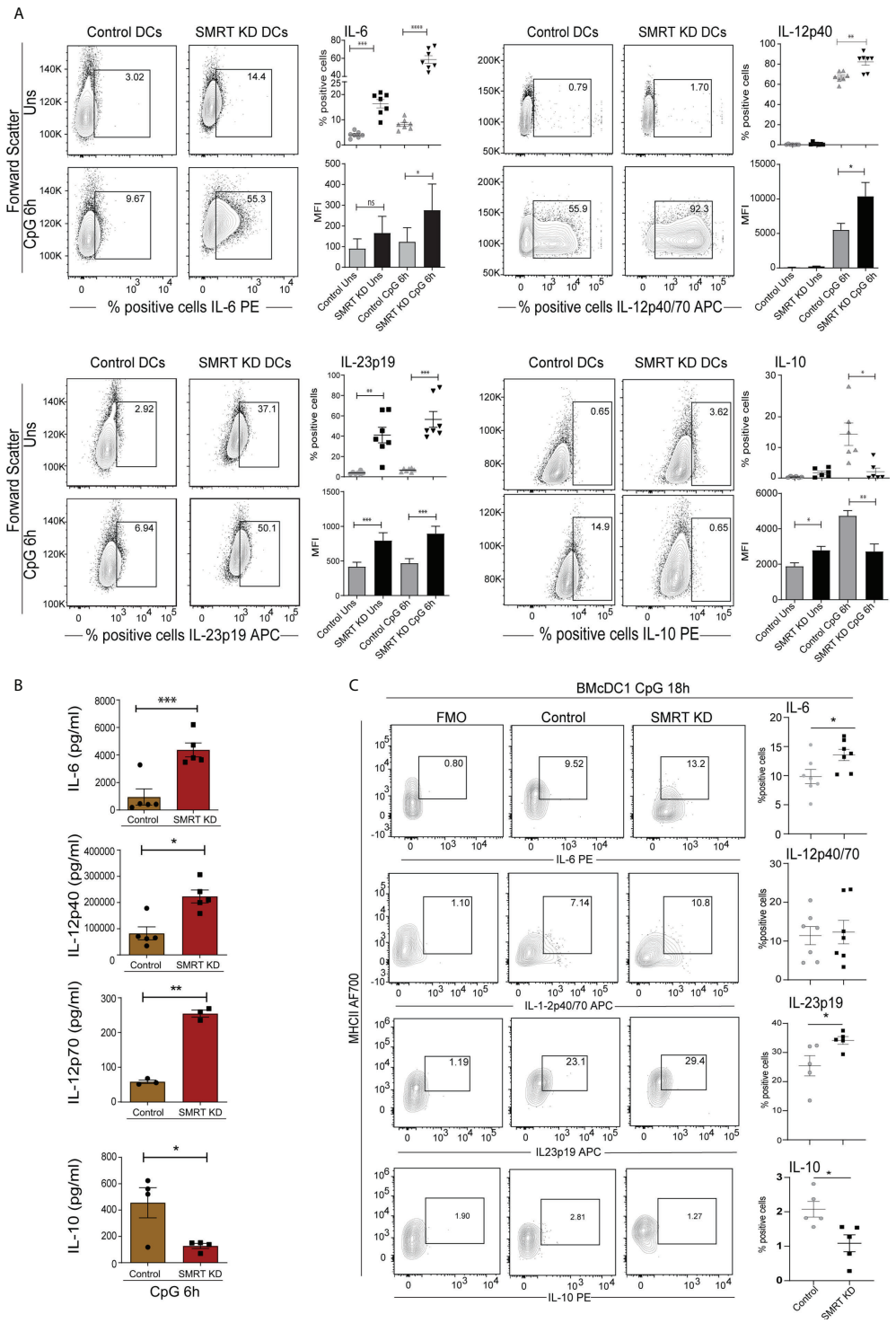

FIGURE 2
Activated SMRT KD cDC1 showed enhanced inflammatory cytokine expression. **(A)** Flow cytometry analysis depicting the intracellular cytokine expression of IL-6, IL-12p40, IL-23p19, and IL-10 in control and SMRT KD cDC1 before and after 6h CpG challenge. Corresponding contour, dot and bar-plots show the percent positive cell population and MFI shifts respectively (n=6-7). **(B)** Bioplex cytokine assay showing the estimation of secreted cytokines IL-6, IL-12p40, IL-12p70 and IL-10 in the culture supernatants of 6h CpG activated control and SMRT KD cDC1 (n=3-5). **(C)** Contour and scatter dot plots depicting percent positive cells expressing of intracellular cytokines IL-6, IL-12p40, L-23p19 and IL-10 in 18h CpG stimulated control and SMRT KD BMcDC1. Gating of the individual cytokines are determined based on their respective FMO controls (n=5-7). *p ≤ 0.05, **p ≤ 0.01 and ***p ≤0.001. p-value has been calculated using two tailed paired **(A, B)** and unpaired **(C)** student's t-test. Data shown in figure is combined from at least three independent experiments **(A–C)**. Error bars represent SEM.

mice with SMRT KD and control cDC1 line. We isolated OT-II T-cells and co-cultured them with OVA pulsed and CpG or pIC activated DCs for 72h to check proliferation and for 96h to check differentiation. For the proliferation experiment we labeled the OT-II T-cells with efluor-670 proliferation dye. We first looked into the proliferation of co-cultured T-cells and found that in SMRT KD cells showed enhanced T-cell proliferation compared to controls (Figures 3A, B and Supplementary Figure 5A). Further we profiled T-cell to understand the impact of control and SMRT KD cDC1 on differentiation of T-cell subtypes. It is well known that IL-6 leads to suppression of forkhead box protein P3 (FOXP3) TF expression, thus repressing Treg differentiation, and along with IL-23 leads to the development of Th17 cells by inducing RORγt expression (27, 28). On the other hand, IL-12p70 is known to upregulate T-bet leading to Th1 differentiation. In our OT-II co-culture experiment, we found a significant increase in percent of $CD44^+$T-$bet^+$$IFN\text{-}\gamma^+$ as well as $CD44^+$$ROR\gamma t^+$$IL\text{-}17^+$ cells supporting enhanced frequency of Th1 and Th17 subtypes respectively in CpG activated SMRT KD cDC1 compared to control DCs (Figures 3C–F). A similar increase in $CD44^+$T-$bet^+$$IFN\text{-}\gamma^+$ cells was observed in pIC stimulated condition as well (Supplementary Figure 5B). To further confirm the increased Th17 polarization, we also checked secretory levels of IL-17 cytokine levels from culture supernatants of co-cultured cells and its level was found to be significantly increased (Figure 3G). We also checked the secretion of IL-13, an important Th2 cytokine, however, no significant difference was observed (Supplementary Figure 5C). Moreover, we also did not observe any significant difference in IL-10, $Foxp3^+$ Tregs or $GATA3^+$ percent positive cells (Supplementary Figure 5D). A representative figure depicting the gating strategy used in co-culture assay to identify $CD3^+$ $CD4^+$ $CD44^+$ T-cells is depicted (Supplementary Figure 5E). First, we gated on FSC-A and $CD3^+$ T-cells followed by doublet discrimination using forward scatter FSC-A and FSC-H. These cells were then gated for $CD4^+$ $CD44^+$. All the downstream analysis was done in these double positive cells.

PBMCs of rheumatoid arthritis (RA) patients depicts decreased *Ncor2* expression

The autoimmune diseases like Rheumatoid Arthritis (RA) have been widely classified as Th1 and Th17 disease and IL-10 expression is also found to be drastically reduced in these patients (29). It had been established earlier that Th1 responses were involved in autoimmune disease. However, work on IFN-γ and $IL\text{-}12^{-/-}$ mice showed that these mice have a high probability of developing collagen-induced arthritis. From this study, the role of Th17 cells has been identified in autoimmunity (30). Therefore, to associate if expression of *Ncor2* is altered in autoimmune disease, we performed RT-qPCR of *Ncor2* from peripheral blood mononuclear cells (PBMCs) of 11 RA patients and 14 healthy donors. Our results demonstrated significantly lower *Ncor2* expression in RA patients compared to their healthy counterparts (Figure 3H). RA patients with disease activity score (DAS) above 4 have been considered in the study. This result suggested that *Ncor2* decrease could be associated with increased inflammatory phenotype in RA disease. All subjects provided informed consent and the study was approved by the Institutional Ethics Committee (KIIT/KIMS/IEC/39/2019).

Co-culture of SMRT KD cDC1 with OT-I $CD8^+$ T-cells increases T-cell cytotoxicity

As we observed significantly increased MHC-I expression in SMRT depleted cDC1, further we were interested to identify if these DCs have the potential to increase cytotoxic activity of $CD8^+$ T-cells. In order to validate this, we isolated $CD8^+$ T-cells from the spleen of OT-I transgenic mice and co-cultured them with control and SMRT KD cDC1. The DCs were first pulsed with SIINFEKL (OVA peptide 257–264) overnight. The pulsed DCs were activated with CpG or pIC for 2h and co-cultured with purified $CD8^+$ T-cells. Next, we checked proliferation after 72h and expression of IFN-γ, perforin and granzyme-B (GrB) after 96h in these co-cultured CD8+ T-cells. For proliferation assay we used eFluor 670 labeled CD8 T-cells. No significant change was observed in the proliferation of co-cultured OT-I CD8+ T-cells (Figures 4A, B). Percent positive $CD8^+CD44^+$ T-cells expressing IFN-γ, granzyme-B, and perforin were significantly upregulated in CpG activated SMRT KD cDC1 as compared to controls (Figure 4C). Similar results were obtained using pIC stimulated conditions (Supplementary Figure 5F). A representative figure depicting the gating strategy used in co-culture assay to identify $CD3^+$ $CD8^+$ $CD44^+$ T-cells is depicted (Supplementary Figure 5G). First, we gated on FSC-A and $CD3^+$ T-cells followed by doublet discrimination using forward scatter FSC-A and FSC-H. These cells were then gated for $CD8^+$ $CD44^+$. All the downstream analysis was done in these double positive cells. Further, we also checked the cytotoxic effect of SMRT KD cDC1 primed CD8 T-cells. We performed an *ex-vivo* killing assay through measuring the viability of B16F10 melanoma cancer cell line. We found an increased cytotoxicity of $CD8^+$ T-cells co-cultured with SMRT KD DCs as compared to control cells indicated by a significant decrease in the viability of B16F10 cells (Supplementary Figure 5H).

10.3389/fimmu.2022.910705

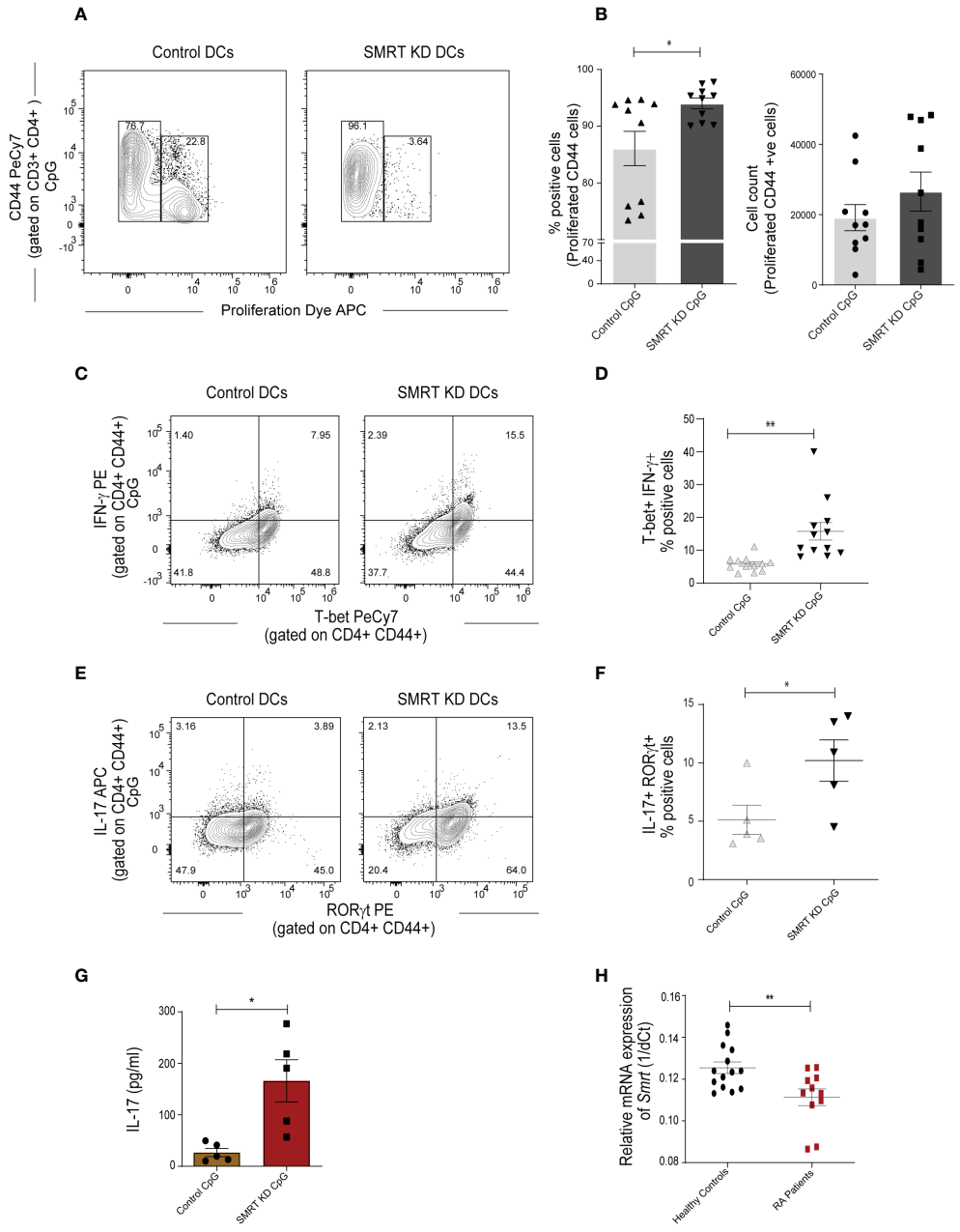

FIGURE 3
SMRT KD cDC1 enhanced Th1 and Th17 cell polarization *ex vivo*. **(A)** Contour plot showing proliferation of effector CD44+ T-cells obtained from co-culture of OT-II T-cells with control and SMRT KD cDC1 pulsed with OVA 323-339 peptide overnight followed by CpG challenge. **(B)** Scatter dot plot with bar showing percent positive and count of proliferated CD44 effector OT-II T cells (n=10). **(C)** Contour plots representing co-cultured OT-II T-cells showing signature transcription factor and cytokine for Th1, T-bet and IFN-γ response in CpG stimulated condition. **(D)** Scatter dot plots representing T-bet and IFN-γ double positive cells in CpG stimulated condition. (n=12). **(E)** Flow cytometry analysis representing contour plots showing RORγt and IL17A as signature transcription factor and cytokines for Th17 subtype generated from co-cultured OT-II T-cells in CpG stimulated condition. **(F)** Scatter dot plots showing RORγt and IL17A double positive cells for Th17 subtype in CpG stimulated condition (n=5). **(G)** Bioplex cytokine assay showing quantification of secretory IL-17 cytokine from supernatant of $CD4^+$ T-cells co-cultured with CpG stimulated control and SMRT KD DCs (n=5). **(H)** RT-qPCR showing relative mRNA expression of *Ncor2* transcript (1/dCt) in RA patients (n=11) and their healthy counterparts (n=14). *p ≤ 0.05 and **p ≤ 0.01. p-value has been calculated using two tailed unpaired student's t-test. Data shown in figure is combined from three independent experiments **(A, B)**, 3-5 independent replicates **(D, F)**, and three independent experiments **(G)**. Error bars represent SEM.

10.3389/fimmu.2022.910705

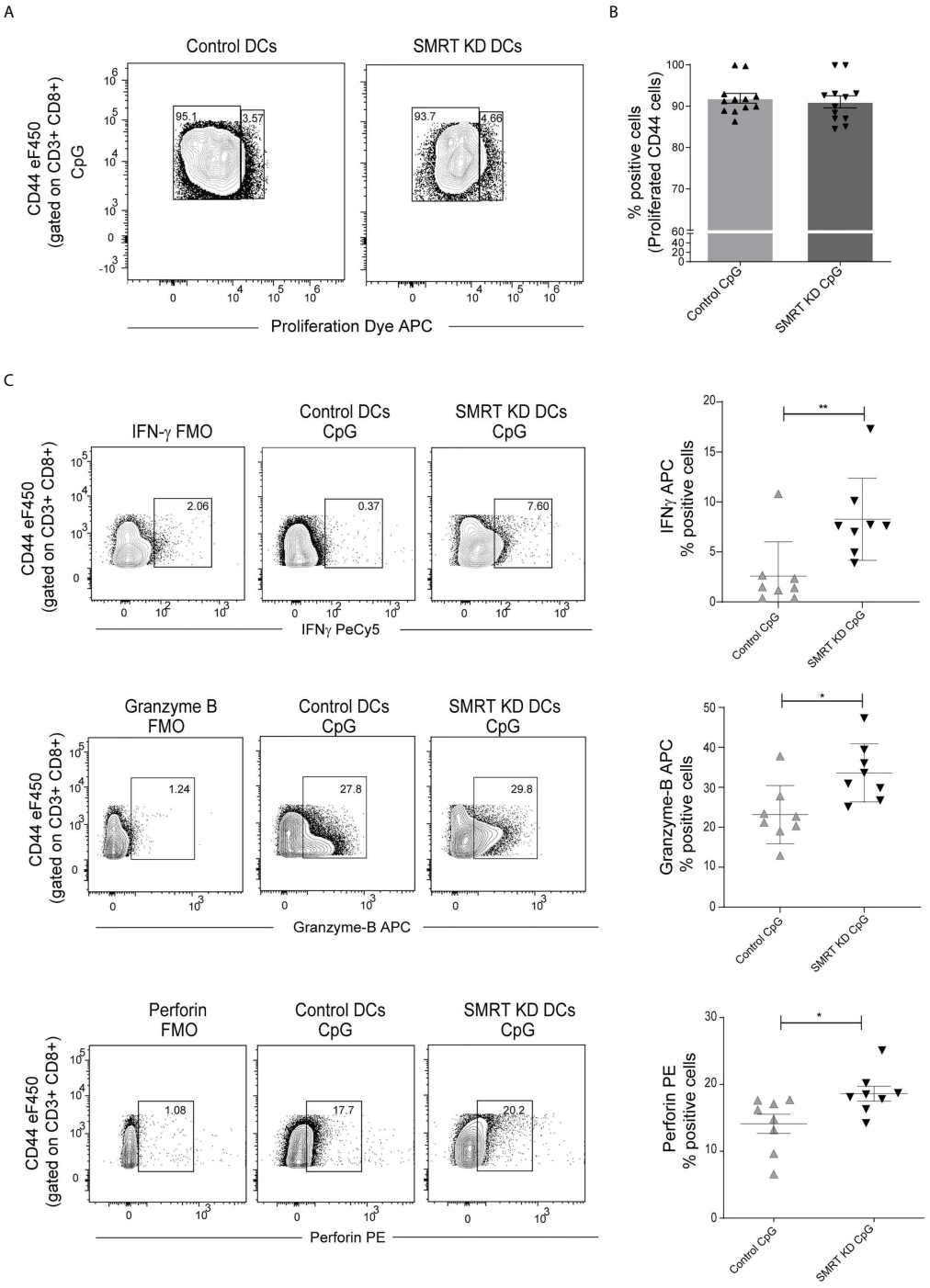

FIGURE 4
SMRT KD cDC1 increased perforin, granzyme, and IFN-γ production *ex vivo* in CD8 T lymphocytes. **(A)** Contour plot showing proliferated CD44 effector OT-I T-cells co-cultured with control and SMRT KD cDC1 pulsed with OVA 257-264 peptide overnight followed by CpG challenge. **(B)** Scatter dot plot with bar showing percent positive of proliferated CD44 effector OT-I T-cells co-cultured with control and SMRT KD cDC1 pulsed with OVA 257-264 peptide overnight followed by CpG challenge (n=12). **(C)** Contour and scatter dot plots depicting percent positive cells expressing IFNγ, granzyme-B, and perforin by OT-I T-cells co-cultured with CpG stimulated control and SMRT KD cDC1. Gating of the individual markers are determined based on their respective FMO controls (n=8). *p ≤ 0.05, **p ≤ 0.01 and ***p ≤0.001. p-value has been calculated using two tailed unpaired student's t-test. Data shown in figure is combined from three independent experiments **(A, B)**, four independent replicates **(C)**. Error bars represent SEM.

Adoptive transfer of CpG pulsed SMRT depleted cDC1 showed enhanced foot pad inflammation in OVA induced Delayed Type Hypersensitivity (OVA-DTH) murine model

We generated an OVA induced Delayed Type Hypersensitivity (OVA-DTH) murine model to study immune modulation by control and SMRT KD cDC1 DCs. Mice were first sensitized with adjuvant (alum) emulsified OVA subcutaneously in the back behind the ears. Control and SMRT KD cDC1 pulsed with OVA for 4h and later activated with CpG for 2h were adoptively transferred at day 14. After one week of adoptive transfer of DCs at day 20, mice were rechallenged with OVA locally in the left footpad to induce hypersensitivity mediated inflammation. The severity of the immune response was examined by measuring footpad swelling every 12h till 72h after the OVA rechallenge (31) (Figure 5A). We found a significant increase in footpad inflammation in mice treated with CpG activated SMRT KD cDC1 compared to control cDC1 and PBS treated animals (Figure 5B and Supplementary Figure 6A). Next, we examined T-cell subtypes in the popliteal and inguinal lymph nodes. Mice injected with SMRT KD DCs exhibited a significantly increased Th1 subtype as shown by IFN-γ, and T-bet positive T-cell population compared to PBS treated group (Figure 5C). At the same time, we found a significantly higher Th17 T-cell population as evident from increased IL-17 and RORγt positive cells in mice injected with SMRT KD cDC1 (Figure 5D). These results showed that decreased SMRT level in DCs generated a very strong inflammatory T cell response in the host.

Adoptive transfer of CpG pulsed SMRT KD cDC1 regresses murine B16F10 melanoma tumor burden

Our observation on enhanced cytotoxic activity of SMRT KD cDC1 led us to examine the antitumor potential of these cells. It has been reported widely that DC vaccine therapy induces oncolytic $CD8^+$ T-cell activity which are specific to tumor associated antigen (TAA) (32). Therefore, to assess the physiological impact of enhanced cytotoxic $CD8^+$ T-cell induced by SMRT depleted DCs, we developed a B16F10 melanoma model in C57BL/6 mice. We hypothesized that animals that received vaccination using inflammatory SMRT KD cDC1 loaded with B16 antigens could resist the increasing tumor burden compared to their control littermates. First, we vaccinated the animals subcutaneously in the left flank with SMRT KD and control cells that were previously pulsed with B16F10 cell lysate to induce immunity against B16F10 tumors. After 3 days, a booster dose was injected. 7 days after the booster dose, we injected $0.1x10^6$ B16F10 cells subcutaneously in mice on the other flank (Figure 5E). Tumor volumes were measured every alternate day starting from 7^{th} to 16^{th} day post tumor development and we found that in the SMRT cDC1 treated group the tumor burden was significantly reduced compared to control DC and PBS treated groups (Figures 5F, G and Supplementary Figure 6B). Further to assess the $CD8^+$ T-cell cytotoxicity, we sacrificed the mice at 16^{th} day post tumor development, dissected the tumors and made single cell suspension by collagenase treatment. We stimulated these cells with PMA/Ionomycin/BFA for 5h and analyzed the $CD8^+$ T-cells using flow cytometry. Further, we checked the percent of CD8 and CD44 cells in the tumor infiltrating lymphocytes. While we found an increased percentage of $CD8^+$ T cells, we did not observe any change in the percentage of $CD44^+$ population in SMRT KD cDC1 treated animals compared to control or PBS groups. (Supplementary Figure 6C). The cytotoxic potential of effector T-cells were significantly increased as indicated by increased frequency of perforin, granzyme-B and IFN-γ percent positive population in SMRT KD cDC1 vaccinated animals as compared to other treatment groups (Figure 5H and Supplementary Figure 6D). Moreover, SMRT KD cDC1 vaccinated animals showed a significant reduction in the weight of excised tumor (Figure 5I). The gating strategy used for the analysis is depicted in Supplementary Figure 6E.

Comparative genomic and transcriptomic analysis of NCoR1 and SMRT in cDC1 showed differential control of STAT3 signaling mediated IL-10 regulation

Recently, we reported that NCoR1 directly binds and strongly represses tolerogenic genes such as *Il10*, *Il27*, *Cd83* and *Socs3* in cDC1. NCoR1 depletion drastically increased the expression of these genes thereby leading to Treg generation *ex vivo* and *in vivo* (25). Contrary to this, here we found that NCoR1 paralog SMRT depleted MutuDC demonstrated drastically increased inflammatory response *in vitro, ex vivo* and *in vivo*. Therefore, we performed comparative genome-wide binding of NCoR1 and SMRT and transcriptomic analysis of NCoR1 and SMRT KD DCs to understand the differential gene regulation by NCoR1 and SMRT. Differential gene expression analysis of SMRT KD versus control cDC1 at 6h CpG stimulation showed 1273 and 934 genes up- and down-regulated respectively (Log2 Fold change >1 and adjusted p-value ≤ 0.01) (Figure 6A; Supplementary File 1). Large number of direct target genes identified using ChIP-seq analysis of SMRT that are upregulated compared to downregulated support its role as a co-repressor (Figure 6B; Supplementary File 2). Further, Ingenuity pathway analysis (IPA) of direct target differentially up regulated genes in SMRT KD condition

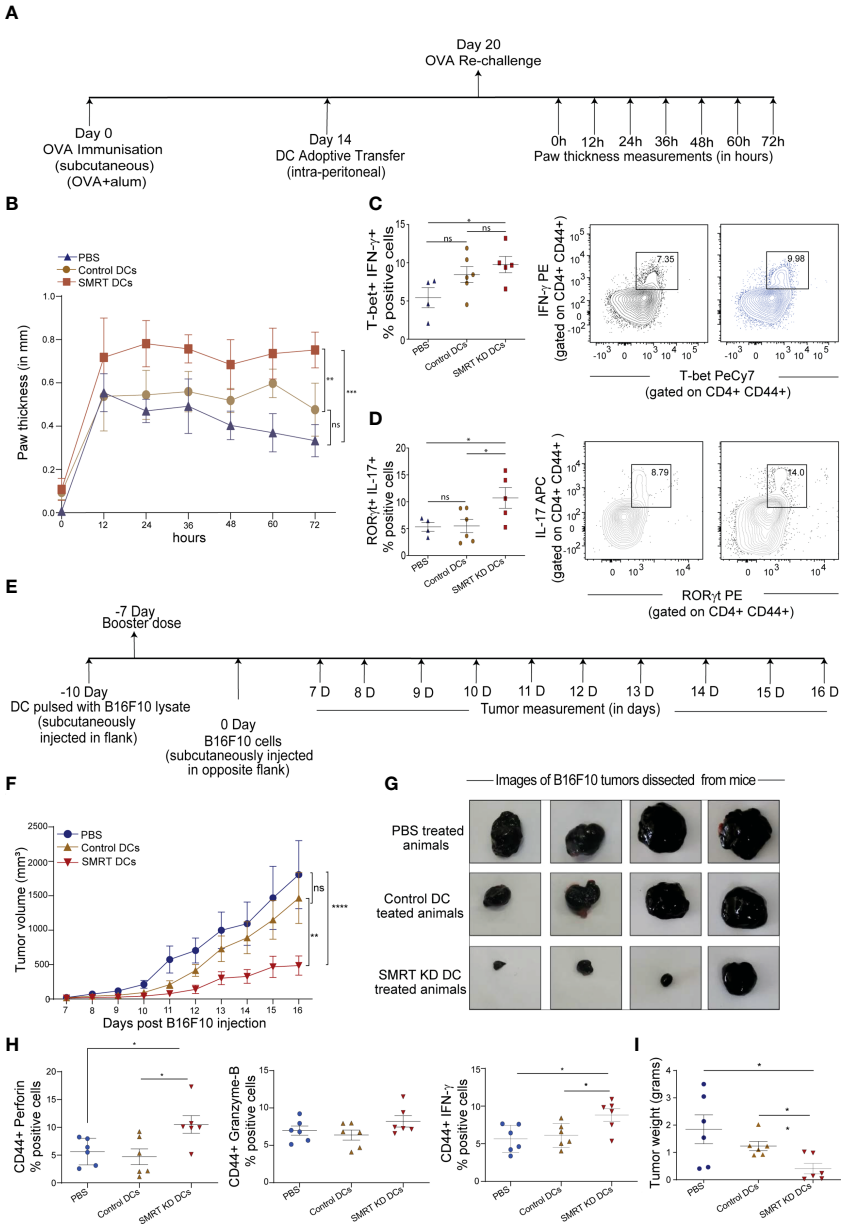

FIGURE 5
Induction of DTH response and tumor regression in C57BL/6 after adoptive transfer of Control and SMRT KD DCs. **(A)** Experimental design depicting DTH model to understand the effect of SMRT KD DCs in comparison to control DCs and PBS treated mice through ova immunization, sensitization and rechallenge followed by measurement of paw thickness. **(B)** Line plot with standard error mean showing footpad swelling till 72h post antigen re-challenge. Footpad swelling was calculated by subtracting the paw thickness (mm) in the right footpad (pbs injection) from left footpad (ova injection) (n=4-6). Statistical analysis was performed between different mice groups. **(C)** Flow cytometry analysis showing scatter dot and contour plot representing Th1 subtype marked by enhanced IFN-γ, and T-bet in SMRT KD DCs isolated from popliteal lymph nodes 72 h post antigen/ova rechallenge (n=4-6). **(D)** Flow cytometry analysis depicting scatter dot and contour plots representing Th17 subtype marked by enhanced IL-17 and RORγt in SMRT KD DCs isolated from popliteal lymph nodes 72 h post antigen/ova rechallenge (n=4-6). **(E)** Experimental design of melanoma model to understand the effect of SMRT KD DCs on tumor regression. Mice were first given tumor vaccination 10 and 7 days prior to tumor injection using DCs pulsed with B16F10 lysates. **(F)** Line plot with standard error mean showing tumor volume that was taken every day starting from 7th day after B16F10 injection till 16 days post tumor rechallenge in PBS, control and SMRT KD DCs injected mice. Tumor volume was calculated as tumor volume = (tumor length x tumor width^2)/2 (n=4-6). Statistical analysis was performed between different mice groups. **(G)** Images showing tumor size isolated from mice at 16 days post B16F10 rechallenge in PBS, control and SMRT KD DCs injected mice (n=4). **(H)** Flow cytometry analysis showing dot plots representing cytotoxic cytokine such as perforin, GrB, IFN-γ from single cell suspension of tumors that were isolated 16 days post B16F10 rechallenge in PBS, control and SMRT KD DCs injected mice (n=6). **(I)** Dot plots showing tumor weight isolated 16 days post B16F10 rechallenge in PBS, control and SMRT KD DCs injected mice (n=6). *p ≤ 0.05, **p ≤ 0.01 and ***p ≤0.001. p-value has been calculated using two-way ANOVA with Tukey's test **(B, F)** and two-tailed unpaired student's t-test. Data shown in figure is combined from two independent experiments **(A–I)**. Error bars represent SEM.

10.3389/fimmu.2022.910705

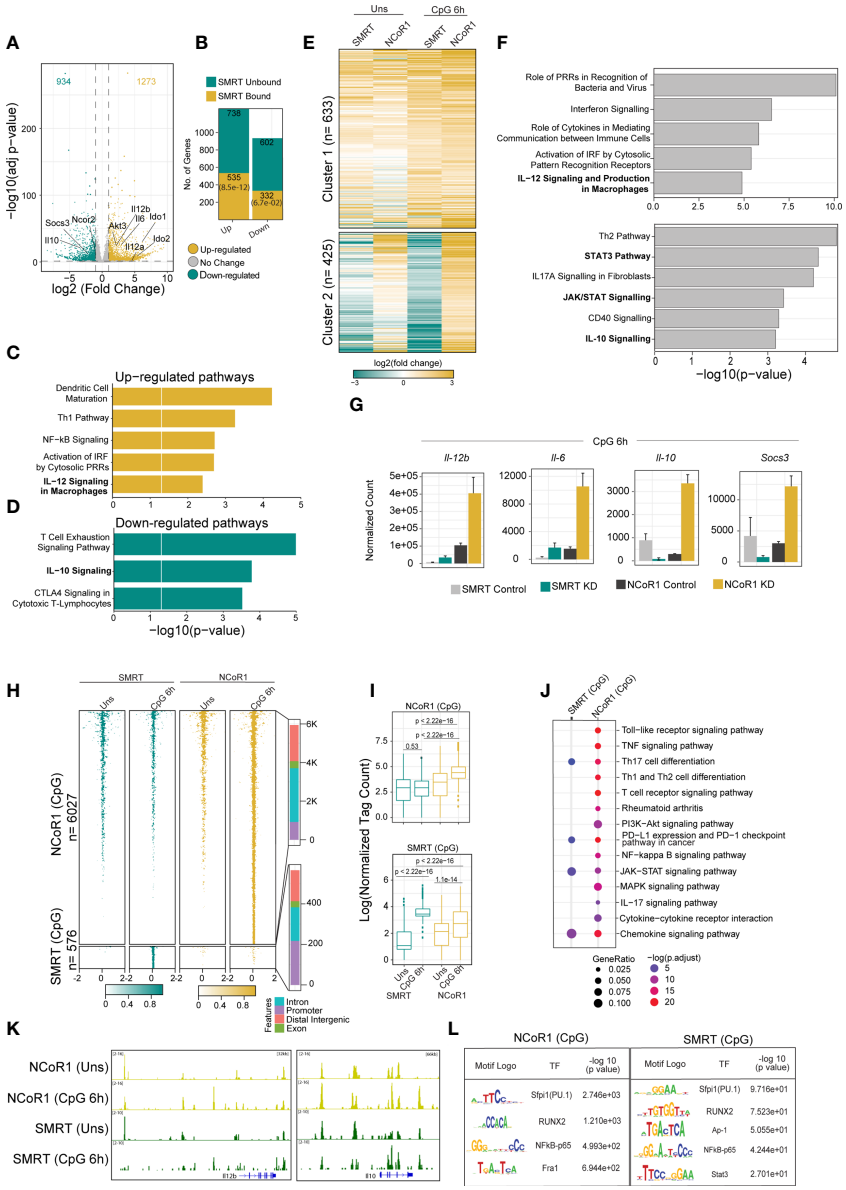

FIGURE 6
Integrative genomics analysis (RNA-seq and ChIP-seq) identified the differential role of SMRT and NCoR1 in regulation of immune response in cDC1. **(A)** Volcano plot showing the differentially expressed genes (DEGs) in SMRT KD cDC1 DCs as compared to control cells after 6h CpG stimulation. 1273 and 934 genes upregulated and downregulated respectively upon SMRT depletion (n=5). **(B)** Bar plot showing the total number of SMRT bound and unbound DEGs in unstimulated and 6h CpG stimulated SMRT KD cDC1 DCs. p-value showing significance of overlap between SMRT bound genes and DEGs. **(C)** Bar plot depicting enriched canonical pathways for the list of SMRT bound upregulated DEGs in 6h CpG activated SMRT KD cDC1 DCs as compared to control cells using Ingenuity pathway analysis (IPA). **(D)** Bar plot depicting enriched canonical pathways for the list of significantly SMRT bound down-regulated DEGs in 6h CpG activated SMRT KD cDC1 DCs as compared to control cells using Ingenuity pathway analysis (IPA). **(E)** Heatmap showing two clusters obtained from K-means clustering of log2 fold change of DEGs upon SMRT and NCoR1 KD compared to control cells in unstimulated and 6h CpG stimulation condition. **(F)** Bar plot showing enriched canonical pathways from IPA for respective clusters shown in Fig 6E. **(G)** Bar plot with standard deviation showing normalized count from DESeq2 of selected genes from enriched pathway for cluster-1 (*Il12b* and *Il6*) and cluster2 (*Il10* and *Socs3*). **(H)** Tornado plot showing ChIP-seq signal (± 2kb to peak center) of differential NCoR1 and SMRT binding sites (NCoR1 CpG and SMRT CpG) in unstimulated and 6h CpG stimulation (1st panel). Bar plot showing the distribution of differential genomic regions based on distance relative to TSS (2nd panel). **(I)** Box plot showing normalized tag count in differential NCoR1 CpG and SMRT CpG cluster. Boxes encompass the 25th to 75th percentile of normalized tag count. Whiskers extend to the 10th and 90th percentiles. Mean difference significance was calculated using the Wilcoxon test. **(J)** Dot plot showing the significantly enriched KEGG terms for genes associated with NCoR1 and SMRT CpG binding clusters shown in Fig 6I. KEGG term enrichment analysis was performed using cluterProfiler R package. **(K)** IGV snapshot showing NCoR1 and SMRT binding on *Il12b* and *Il10* gene loci. **(L)**. Table showing transcription factor motifs that were significantly enriched (P-value< 1e-10) in differential NCoR1 CpG and SMRT CpG clusters.

depicted up-regulation of inflammatory response pathways such as IL-12 signaling (Figure 6C; Supplementary File 3). However, in contrast to NCoR1, SMRT KD showed down-regulation of IL-10 signaling pathway at 6h CpG stimulation (Figure 6D; Supplementary File 3). Next, principal component analysis of NCoR1 and SMRT KD cDC1 RNA-seq clearly showed SMRT KD unstimulated and 6h CpG stimulated condition cluster separately from respective NCoR1 samples (Supplementary Figure 7A). Interestingly, in unstimulated condition the number of differentially regulated genes (up-regulated (n=1060) and down-regulated (n=805)) are much higher in SMRT KD condition as compared to NCoR1 KD DCs (Supplementary Figures 7B, C; Supplementary File 1). The PCA analysis and difference in the number of differentially expressed genes (DEGs) between SMRT and NCoR1 KD indicated a differential control of gene regulation by SMRT and NCoR1 in cDC1. To identify gene sets showing different pattern of expression after NCoR1 and SMRT KD, we performed unsupervised K-means clustering of DEGs based on log2 fold change and identified six clusters (Figure 6E and Supplementary Figure 7D; Supplementary File 4). The genes in cluster-1 showed increased fold change in both NCoR1 and SMRT KD and depicted enriched pathways such as "Interferon signaling", "Activation of IRF by cytosolic pattern recognition receptors", "IL-12 signaling and production in macrophages". On the contrary, cluster-2 genes showed differential regulation between SMRT and NCoR1 KD 6h CpG condition and pathways enriched were "Th2 pathway", "STAT3 pathway", "IL-17-A signaling" and "IL-10 Signaling". (Figure 6F; Supplementary File 5). Other clusters (3-6) genes also showing similar or differential effect upon NCoR1, and SMRT KD were enriched for cytokine signaling pathways terms such as "IL-8", "IL-7" and "IL-15" signaling (Supplementary Figures 7D, E; Supplementary File 2). These observations clearly suggested that inflammatory immunogenic response genes such as *Il12b* and *Il6* are repressed by both NCoR1 and SMRT, however, the regulatory genes like *Il10*, *Socs3* are strongly repressed by NCoR1 only (Figure 6G). Apart from the above listed gene, we also found other reported positive regulator of pro-inflammatory genes such as *Zbtb20* is upregulated and positive regulator of tolerogenic program such as *Wnt11*, *Clec4a2* is downregulated in SMRT KD cDC1 (Supplementary File 1) (33–36). As IL-10 is a physiologically important cytokine and well reported to perturb the inflammatory response towards immune-tolerance, understanding mechanistic control of differential IL-10 regulation by SMRT and NCoR1 was interesting (37). We compared the cistrome of SMRT and NCoR1 before and after 6h CpG activation (~13,000 peaks) (Supplementary Figure 8A). In SMRT, 40% (≈5000) of the total bound sites are distributed at the promoter-proximal (± 1kb to transcriptional start site (TSS)) regions whereas only 18% of NCoR1 peaks (≈2000 peaks) were found at promoter-proximal regions (Supplementary Figure 8B). Besides, differential binding of NCoR1 and SMRT peaks identified NCoR1 dominant (12,473), common NCoR1-SMRT (5949) and SMRT dominant (2707) genomic regions (Figures 6H, I and Supplementary Figure 8C). SMRT dominant regions showed predominance in promoter-proximal regions compared to NCoR1 dominant and common NCoR1-SMRT regions distributed mostly in intronic or distal intergenic regions (Figure 6H, and Supplementary Figure 8C). This further strongly suggested that SMRT mostly regulate the genes through promoter-proximal binding, whereas NCoR1 and common NCoR1-SMRT bound genes are regulated through far-distal regulatory elements. Further, KEGG pathway analysis of genes associated with genomic regions showing CpG dependent increase in NCoR1 or common NCoR1-SMRT binding is significantly enriched for "Th1 and Th2 pathway", "Th-17 signaling pathway", "NFkB signaling pathway", and "JAK-STAT signaling pathway" (Figure 6J and Supplementary Figure 8D, Supplementary File 6). Co-occupancy of NCoR1 as well as SMRT on both inflammatory (*Il12b*) and tolerogenic genes (*Il10*) at several proximal or distal regions to TSS after CpG activation shows involvement of both the repressor in regulating immune response genes (Figure 6K). To identify the putative transcription factors (TFs) recruited before and after 6h CpG activation at these co-repressors bound genomic regions, we performed *de novo* motif enrichment analysis and found that PU.1, RUNX2 and Jun-Fos/AP1 TFs motifs were enriched at almost all NCoR1, and SMRT bound genomic regions showing enrichment in unstimulated or 6h CpG activation condition. Interestingly, NFkB motifs were found to be enriched at CpG dominant NCoR1, dominant SMRT and common NCoR1-SMRT binding. IRF8 and IRF4 motifs were enriched at dominant NCoR1 and common NCoR1-SMRT regions in both unstimulated and 6h CpG activation conditions respectively (Figure 6L and Supplementary Figure 8E). The above enriched motifs corroborate with our previous finding on NCoR1 bound regions (25). Apart from the above motifs we found an enrichment of STAT3 motif at CpG dominant common NCoR1-SMRT and CpG dominant SMRT genomic regions. Since member of NFkB family and Stat3 transcription factor plays an important role in regulation of inflammatory (*Il12b*, *Il6*) and tolerogenic (*Il10*, *Socs3*) gene expression, to further understand downregulation of tolerogenic genes, we checked expression of other genes associated with Jak-Stat signaling pathway. We found a clear difference in regulation of several other Jak-Stat signaling which is downregulated in SMRT KD DCs but not in NCoR1 KD DCs (Figure 7A, B). Overall, our comparative genomic and transcriptomic analysis

10.3389/fimmu.2022.910705

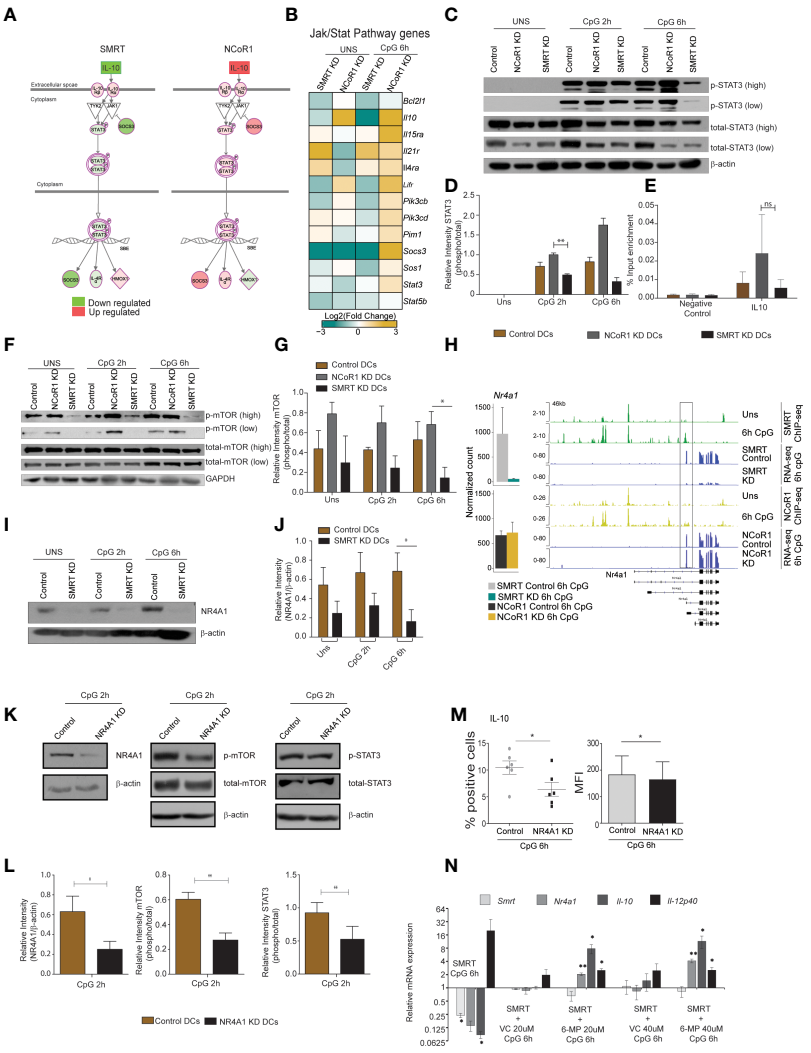

FIGURE 7
Nurr-77, mTOR, Stat3 signaling regulates IL-10 expression in SMRT KD cDCs. **(A)** Illustration of Jak/Stat Signaling pathway from Ingenuity pathway analysis with mapped expression of genes. (Red and green indicate high and low expression respectively). **(B)** RNA-seq analysis showing heatmap showing Log2 (fold change) of all the genes in KEGG Jak-Stat signaling term shown in Fig 6L. **(C)** Western blot depicting phospho-STAT3, total STAT3, and β-actin protein levels in unstimulated and 2h and 6h CpG stimulated control, NCoR1 KD, and SMRT KD cDC1. **(D)** Bar plot with standard error mean from densitometric analysis depicting normalized intensity of phosphorylated STAT3 bands in control and KD cDC1. Housekeeping gene β-actin was used as loading control (n=3). **(E)** Bar plot with standard error mean showing % input enrichment from ChIP-qPCR of phospho-STAT3 on IL-10 enhancer region in 2h CpG stimulated control, NCoR1 KD, and SMRT KD cDC1. (n=3) **(F)** Western blot depicting the levels of phosphorylated mTOR, total mTOR, and GAPDH in unstimulated, 2h, and 6h CpG stimulated control, NCoR1 KD, and SMRT KD cDC1. Housekeeping gene GAPDH was used as loading control. **(G)** Bar plot with standard error mean from densitometric analysis depicting normalized intensity of phosphorylated mTOR bands in control and KD cDC1. Housekeeping gene GAPDH was used as loading control (n=3). **(H)** Bar plot with standard deviation showing normalized count of *Nr4a1* gene in NCoR1 and SMRT KD cDC1 with their respective matched controls in 6h CpG stimulation. IGV snapshot showing SMRT and NCoR1 binding at *Nr4a1* gene loci in control unstimulated and 6h CpG stimulated DCs along with RNA-seq in control, SMRT KD and NCoR1 KD DCs in 6h CpG stimulation condition. **(I)** Western blot depicting the levels of NR4A1 and β-actin in unstimulated, 2h, and 6h CpG stimulated control and SMRT KD cDC1 (n=3). **(J)** Bar plot with standard error mean from densitometric analysis depicting the normalized intensity of NR4A1 bands in KD and control cells. Housekeeping gene β-actin was used as loading control (n=3). **(K)** Western blot depicting the levels of phospho-mTOR, total mTOR, phospho-STAT3, total STAT3, NR4A1, and β -actin in 2h CpG stimulated control and NR4A1 KD cDC1. **(L)** Bar plot with standard error mean from densitometric analysis depicting the normalized intensity of phosphorylated-mTOR, phosphorylated-STAT3, and NR4A1 in 2h CpG stimulated control and NR4A1 KD cDC1. Housekeeping gene β-actin was used as loading control (n=4). **(M)** Percent positive cells and MFI depicting flow cytometry analysis of the anti-inflammatory cytokine IL-10 in 6h CpG stimulated control and NR4A1 KD DCs. (n=6) **(N)** Relative transcript expression of *Ncor2*, *Nr4a1*, *Il10*, and *Il12b* transcript in 6h CpG-B stimulated SMRT KD, CpG along with vehicle treated SMRT KD and CpG along with 6-MP treated SMRT KD DCs as estimated by RT-qPCR (n=3). *p ≤ 0.05 and **p ≤ 0.01. p-value has been calculated using two tailed paired student's t-test. Data shown in figure is combined from 3-4 independent experiments **(C–L)**, four independent experiments **(M)**, and three independent replicates **(N)**. Error bars represent SEM. "ns" stands for non significant.

suggest that SMRT KD DCs show dysregulation of STAT3-IL-10 axis in contrast to NCoR1 KD DCs.

SMRT mediated down-regulation of NR4A1 inhibited mTOR-STAT3 signaling leading to IL-10 suppression

STAT3 TF plays a central role in Jak-Stat signaling and regulated expression of *Il10* and *Socs3*. We also found NFkB inhibitory genes such as *Nfkbia* and *Tnfaip3* were also downregulated after 6h CpG stimulation in SMRT KD cDC1. First to confirm the differential regulation of p-STAT3 in NCoR1 and SMRT, we did western blotting for p-STAT3 in NCoR1 KD, SMRT KD and control cDC1 at 0h, 2h, and 6h after CpG activation. We found that p-STAT3 is down-regulated in SMRT KD cDC1 compared to control cells whereas it was upregulated in NCoR1 depleted DCs (Figures 7C, D). It is well reported that STAT3 binds to the *Il10* gene to regulate its expression (38). We also checked STAT3 binding on *Il10* gene at 0h and 6h LPS stimulation in BMDCs (Supplementary Figure 8F) (39). Therefore, we performed chromatin immunoprecipitation (ChIP) for p-STAT3 followed by RT-qPCR to infer the binding of p-STAT3 on *Il10* gene after 2h CpG challenge in control, NCoR1 KD, and SMRT KD cDC1. We observed reduction in p-STAT3 binding on *Il10* in SMRT KD DCs relative to control DCs whereas on the other side, the binding was found to be enhanced in NCoR1 KD cells as compared to control cells (Figure 7E). Moreover, to understand the upstream control of STAT3 signaling in these DCs we looked into the literature and identified that mTOR has been reported to control STAT3 activation and mTOR on the other hand is regulated by nuclear receptor NR4A1 also known as NURR-77 (40, 41). We first checked the regulation of phospho-mTOR (p-mTOR) in NCoR1 and SMRT depleted cDC1 and found that p-mTOR is upregulated in NCoR1 KD cDC1 whereas it is drastically reduced after SMRT depletion (Figures 7F, G). In addition, we found differential regulation of *Nr4a1* (Nur77) in SMRT and NCoR1 depleted DCs. SMRT KD leads to downregulation of *Nr4a1* while NCoR1 KD has no significant effect on expression of *Nr4a1* (Figure 7H). Further we checked direct binding of NCoR1 and SMRT on *Nr4a1* in ChIP-seq data using IGV browser and observed that SMRT but not NCoR1 binds at the TSS of the transcript that is expressed in DCs after 6h CpG activation (Figure 7H). We also confirmed this observation by assessing the NR4A1 protein expression in SMRT depleted and control cDC1 before and after 2h and 6h CpG activation and found that NR4A1 is significantly down-regulated in SMRT KD DCs as compared to control cells (Figures 7I, J). Further to confirm that NR4A1 indeed is controlling the STAT3 signaling through mTOR in SMRT depleted cells, we generated a stable NR4A1 KD and empty vector transduced (control) cDC1 using NR4A1 lentiviral shRNA to confirm its role in mTOR-Stat3-Il-10 signaling. In stable NR4A1 depleted mutu-cDC1 we first confirmed the depletion of NR4A1 by western blotting and found it to be significantly reduced (Figures 7K, L). Then we checked p-mTOR and phospho-STAT3 (p-STAT3) after 2h CpG activation which were found to be significantly reduced in NR4A1 depleted cDC1 compared to control cells (Figures 7K, L). Moreover, in these NR4A1 depleted DCs we also confirmed significant reduction of IL-10 percent positive cells and corresponding MFI shifts upon 6h CpG treatment (Figure 7M). Moreover, we also tried to over-express NR4A1 ORF transiently in SMRT depleted cDC1, but we didn't manage to perform this analysis as the cells were not in good condition after transduction of overexpression plasmids. Therefore, we used an alternative approach. It has been reported that 6-mercaptopurine (6-MP) induces the expression of NR4A1 in cells (19). Therefore, we used 6-MP to enhance the expression of *Nr4a1* in SMRT depleted cDC1 to see if it can complement the *Il10* expression. We found that 6-MP treatment enhanced the expression of *Nr4a1* in SMRT depleted cDC1 leading to an increase in expression of *Il10* (Figure 7N). These results confirmed that SMRT KD mediated down-regulation of NR4A1 resulted in reduction of STAT3 activation and thereby decreased IL-10 levels and enhanced inflammatory phenotype of cDC1.

Discussion

Dendritic cells make a strong connecting link between innate and adaptive immunity. Besides, a fine balance of DC signals is pertinent for development of an optimal immunogenic versus tolerogenic response to protect from autoimmune diseases and opportunistic infections. Though signaling pathways controlling one response versus another have been widely explored, how this balance is fine-tuned in DCs is interesting to understand for developing DC based therapies. We recently reported that NCoR1 directly binds and represses the transcription of regulatory genes like *Il10, Cd274, Cd83* and *Il27* and its loss of function in DCs enhanced Treg development (25). Similarly, it has been demonstrated earlier by Li. et al. that macrophage specific depletion of NCoR1 in high fat induced obese mice derepresses LXRs which generates anti-inflammatory response through increased expression of genes involved in fatty acid biosynthesis (42). In contrast to NCoR1 in this study we have shown that SMRT depletion in cDC1 leads to increase in expression of pro-inflammatory genes (*Il12a, I12b, Il6, Il23a*) and decreased tolerogenic genes such as *Il10* and *Socs3*. Expression of these genes enhanced Th1 and Th17 frequency along with increased cytotoxic T-cell when primed with these DCs. The paradoxical effect of these two proteins, NCoR1 and SMRT, has been reported to be dependent on other interacting proteins in the co-repressor complex. As demonstrated by *Fan et. al*, the differential role of NCoR1 and SMRT is attributed to

GPS2, a component of the corepressor complex which also contains HDAC3, NCoR1, SMRT, TBL1, and TBLR1 (43). Macrophage specific deletion of GPS2 or SMRT leads to increased pro-inflammatory gene expression while NCoR1 or HDAC3 depletion leads to enhanced anti-inflammatory effect (42, 43). An extremely crucial observation in this study was that SMRT but not NCoR1 depletion hampered GSP2 recruitment to its target gene Ccl2, an inflammatory chemokine. Thus, GSP2 has been linked to SMRT, but not NCoR1, functionally. These results support the fact that NCoR1 and SMRT are crucial for inflammatory versus anti-inflammatory responses in immune cells. To understand this further, we performed comparative genomic analysis of NCoR1 and SMRT depleted DCs and found that they differentially regulate mTOR-STAT3 signaling pathway leading to tight regulation of IL-10. Overall, our analysis for the first time identified a fine switch that could be targeted to modulate inflammatory versus tolerogenic programs in cDC1 DCs.

IL-10 is a potent anti-inflammatory cytokine that can limit host inflammatory response to pathogens thereby preventing host from damage. Dysregulated IL-10 is involved in enhanced immune-pathology and associated with development of auto-immune diseases (44). The expression of IL-10 is dependent on STAT3 TF and it has been reported that STAT3 regulates *Il10* expression by binding to its regulatory region (13, 45). At the same time, the positive feedback loop from IL-10 through STAT3 maintains its sustained expression. Immune-profiling analysis of NCoR1 and SMRT depleted cDC1 depicted significant upregulation of IL-10 in NCoR1, whereas it was drastically down-regulated in SMRT KD condition. When we looked at STAT3 regulation employing the integrative genomic analysis, it clearly showed significant down-regulation of STAT3 pathway in SMRT KD cDC1. In contrast to this it was significantly upregulated in NCoR1 KD condition. Moreover, we found that there is increased binding of STAT3 on *Il10* in NCoR1 as compared to SMRT depleted cells. Overall, it is quite intriguing that two highly homologous co-regulators showed this differential regulation of an important pathway i.e., STAT3 and thereby IL-10 expression. Apart from STAT3 there are other transcription factors like Sp1/Sp3, NF-kB, c-Maf, Smad4 that also exhibit a similar phenomenon in macrophages. However, studies showed that there is no increased binding of Sp1/Sp3 on *Il10* promoter in murine BMDCs (46). We further explored to identify the mechanisms for differential regulation of STAT3 signaling. It has been reported that mTOR activates STAT3 (47) and we found that p-mTOR is up-regulated in activated NCoR1 KD cDC1 whereas it is drastically reduced in SMRT KD cDC1.

Furthermore, we observed that SMRT depleted DCs have sustained and increased expression of pro-inflammatory cytokines like IL-6, IL-12 and IL-23 thereby leading to enhanced development of Th1 and Th17 cells *ex-vivo* and *in-vivo* animal models. When we analyzed our global transcriptome data, we found that *Socs3* is significantly downregulated along with negative regulators of NFkB signaling such as *Nfkbia* and *Tnfaip3*. It has been widely reported that SOCS3 depletion enhances the Th1 and Th17 polarizing cytokine release in DCs (48). The *Socs3* down-regulation was observed only in activated SMRT KD cDC1 after 6h activation, which suggested that the initial events of IL-10 and STAT3 decrease through down-regulation of mTOR activity are somehow leading to SOCS3 decrease. To our surprise, we found that SOCS3 and STAT3 both are down regulated in SMRT KD cDC1, as in several reports it has been documented that decreased SOCS3 favors enhanced STAT3 (49). We hypothesize that it could be due to the dynamic time dependent regulation of STAT3 and SOCS3 in CpG activated SMRT KD cells.

Moreover, as we observed a drastic decrease of p-mTOR in unstimulated SMRT KD cDC1, we looked into the regulators of mTOR. We found an interesting nuclear receptor *Nr4a1* to be significantly down-regulated in RNA-seq data of unstimulated and CpG activated SMRT depleted DCs. NR4A1 has been reported to positively regulate mTOR activity and thereby STAT3 phosphorylation and IL-10 expression (50). It is also shown that deficiency of NR4A1 leads to enhanced production of IL-6, TNF-α, and IL-12 in both human and murine dendritic cells (19). We showed that indeed NR4A1 expression was down-regulated supporting our finding in SMRT depleted DCs. It has been reported that ASC-2 and SMRT lead to transactivation and repression of NR4A1 respectively (21). We looked into the expression of ASC-2 (*Ncoa6*) and CaMKIV (*Camk4*) transcripts in SMRT KD cells but surprisingly we didn't observe any significant change or downregulation. As we observed that SMRT KD downregulated a large number of genes even in unstimulated condition, it is plausible that an important NR4A1 transactivation factor is also down-regulated leading to its decreased expression. On the other side, complementing *Nr4a1* in SMRT depleted cDC1 by treating with 6-MP rescued *Il10* expression.

In an *in-vivo* physiological system, the maintenance of Th1, Th17, and Th2 balance depends on a number of factors including antigen presentation by MHC-II, co-stimulation and differential cytokine production (51). To address whether the manipulation of DCs by SMRT KD towards an enhanced Th1 and Th17 type responses could deliver a long term functional and effector memory response, we developed DTH and B16F10 melanoma models. The SMRT depleted and control DCs were adoptively transferred and perturbation in DTH responses and B16F10 melanoma progression was observed. We found that SMRT depleted DCs have potential to enhance Th1 and Th17 type responses and thereby DTH enhancement in animals. At the same time, oncolytic $CD8^+$ T-cell activity was enhanced leading to reduced tumor burden in animals. Furthermore, it has been widely reported that in autoimmune diseases such as RA and Multiple Sclerosis (MS) enhanced Th1 and Th17 cells result in inflammatory symptoms (52). As we observed enhanced Th1 and Th17 response by SMRT depleted DCs we found

significantly reduced SMRT expression in mononuclear cells of RA patients as compared to controls. Therefore, it is further interesting to explore if SMRT co-repressor has some potential association with autoimmune pathogenesis and can be used as a target for immunotherapy.

Limitations of the study

We have studied the role of SMRT in cDC1 through shRNA mediated knock-down. The effect observed *in vitro* and *ex vivo* in the SMRT depleted cDC1 could provide further validation through overexpression of the co-repressor, however, owing to the high molecular weight of the SMRT protein, the overexpression in cDC1 is challenging.

The correlation of *Ncor2* expression with inflammatory phenotype in RA patients is studied in PBMCs and not in cDC1 specifically. Although, *Ncor2* expression specifically in cDC1 of RA patients can be interesting, however, the cell numbers make it limiting. To understand the functional relevance of SMRT in human cDC1, large RA patient cohort data need to be studied to correlate the expression of SMRT with inflammatory phenotype that is well reported in RA patients. Additionally, we have studied the role of SMRT on cDC1 cells however an elaborative study of the corepressor in other DC subtypes can further substantiate the importance of SMRT.

Materials and methods

Mice

C57BL/6 wild type mice bred and maintained at ILS animal facility. OT-II and OT-I transgenic mice (gifted by Prof. Hans Acha-Orbea, University of Lausanne) and C57BL6

Flt3 transgenic mice (gifted by Ton Rolink) were transported from SWISS. All the animal experiments were performed after getting due approval from the institutional animal ethics committee (ILS/IAEC-164-AH/AUG-19) and (ILS/IAEC-123-AH/AUG-18).

Cell lines

The CD8α+ MutuDC cell line used in this study has been gifted by Prof. Hans Acha-Orbea's group. The cell lines were maintained in culture at 37°C in a humidified incubator with 5% CO2. Cells were cultured in complete IMDM-glutamax medium with all buffered conditions as reported previously. These cells show resemblance in expression of surface markers and mimic splenic *ex vivo* immature CD8α$^+$ DCs as shown by extensive characterization done by Prof. Hans Acha-Orbea's group (26).

B16F10 cell line were obtained from Dr. Shantibhushan Senapati Lab and maintained and cultured in DMEM media at 37°C in a humidified incubator with 5% CO2.

For *in vitro* experiments, the DCs were plated in 12- or 6-well plates at a density of 5×10^5 or 1×10^6 cells/ml overnight. The cells were then challenged with different activation media containing TLR9 agonist CpG-B at a concentration of 1ug/ml, TLR3 agonist pIC at 2ug/ml for 2, 6 and 12h. For performing RT-qPCR analysis the cells were washed in the plate once with PBS followed by addition of RNA-later (LBP) lysis buffer for lysis of cells. The plates were then stored at −80°C until further RNA isolation and processing of samples.

Generation of stable SMRT KD CD8α$^+$ MutuDCs

For generating stable SMRT knockdown and their comparative control DC cells, lentiviral vector pLKO.1 (Sigma) containing three different sigma mission shRNA for *Ncor2* were picked targeting chromosome 5 on mouse genome against exons 48, 19, and 14 respectively (Key Resources Table). Viral particles packaged with shRNA expressing transfer plasmids were produced in 293T cells using Cal-Phos (CaPO4) mammalian transfection kit according to an optimized protocol. We used a 2nd generation lentiviral system which included PCMVR and PMD2G as packaging and envelope plasmids respectively. Human embryonic kidney (HEK) 293T cells were transfected with transfer plasmids containing three different *Ncor2* shRNAs or control shRNAs along with pCMVR8.74 and pMD2G. After 12–14h the culture medium was replenished and supernatant containing viral particles were collected after 24h in 50 ml conical tubes. Viral particle-containing culture supernatant was concentrated using ultracentrifugation at 50,000g at 16°C for 2h and preserved at −80°C in small aliquots. For transduction of shRNA containing viruses in CD8α$^+$ cDC1 MutuDC lines, the cells were plated at a density of 1.5×10^5 cells/well of 12 well plate followed by transduction with virus particles containing supernatant. The media was replaced with fresh media after 12h of virus incubation with DCs followed by addition of 1 µg/ml puromycin selection medium after 72 h of media replacement for stable KD cells.

RNA isolation and RT-qPCR

The extraction of RNA was done using NucleoSpin RNA Plus miniprep kit (Machery Nagel). Briefly, cells were preserved in LBP lysis buffer in −80°C and thawed by placing the plates/tubes on ice. Total RNA was isolated according to the manufacturer's protocol. RNA concentration was estimated by nanodrop (Thermo) and then 1-2 µg of total RNA was used to prepare cDNA using high-capacity cDNA Reverse Transcriptase

kit (Applied Biosystems). Quantitative PCR was performed using SYBR Green master (Roche) and PCR amplification was monitored in real-time using LightCycler-480 Instrument. Primer oligonucleotides for qPCR were designed using the universal probe library assay design system and the primer pairs used are listed in Key Resources Table. Primers were optimized for linear and single product amplification by performing standard curve assays.

Flow cytometry

We performed flow cytometry analysis using the well-established surface and intracellular (IC) staining protocols (25). 5 x 10^5 and 1.5 x 10^6 cells were seeded for surface and IC staining respectively. Cells were either left unstimulated or stimulated with CpG or pIC for 6h. For staining the cells were dissociated and washed with FACS buffer (3% FCS in 1X PBS, 5 mM EDTA). After washing, fluorochrome conjugated antibodies for proteins of interest were added to the cells as a cocktail in the staining buffer. For surface staining cells were stained in FACS buffer for 30 min in dark at 4°C. For IC staining of cytokines the cells were first fixed with 2% paraformaldehyde for 20 min followed by permeabilization using 1x permeabilization buffer (eBiosciences). The fixed and permeabilized cells were then resuspended in IC staining buffer and stained with fluorochrome tagged antibodies for selected cytokines. For optimal staining the cells were incubated with antibodies for 30 min in dark. After incubation the cells were washed twice with FACS wash buffer and then acquired for differential expression analysis using LSRII fortessa flow cytometer (BD Biosciences). The acquired data was analyzed using FlowJo-X software (Treestar). Antibodies used for flow cytometry experiments are listed in the Key Resources Table.

Bio-plex assay for cytokine quantitation from cell culture supernatants

Bio-Plex assay (multiplex ELISA) was used to estimate the cytokine levels secreted in the cell culture supernatants of SMRT KD and control DC and BMcDC1 after 6 h of CpG stimulation according to previous reports (25). After culture, the supernatants were stored at −80°C in small aliquots until analysis. Cytokine levels were estimated using 23-plex-mouse cytokine assay kit following the vendor recommended protocol (Biorad).

Generation of bone marrow derived DCs for *ex-vivo* studies

Six to eight-week-old female C57BL/6 mice were killed by cervical dislocation and disinfected using 75% ethanol (25). In short, the tibias and femurs were removed under sterile conditions, then soaked in RPMI-1640 medium supplemented with 10% FBS. Cells from both ends of the bone were flushed out with a needle of 1-mL syringe from the bone cavity into a sterile culture dish with RPMI-1640 medium. The cell suspension in the dish was collected and centrifuged at 350g for 5 min, and the supernatant was discarded. The cell pellet was suspended with a 1x RBC lysis buffer (Tonbo) for 5-10 min on ice. Cell clumps were then passed through a 70µm strainer to obtain single cell suspensions. The lysed cells were washed once with RPMI-1640, counted and used for differentiation into DCs.

We followed a well-established protocol for differentiation of BMDCs with slight modifications. The cells, suspended in RPMI-1640 medium supplemented with 10% FBS, were distributed into 6-well plates at a density of 1 × 10^6 cell/ml/well. Subsequently, 1µl/ml of FLT3L containing sera was added into the medium. The cells were cultured at 37°C in an incubator containing 5% CO2 and left untouched for 7 days. On day 7, the suspended and loosely attached cells were collected.

The cells were plated into a 12-well plate for lentiviral transduction using concentrated viruses at a density of 1 x 10^6 cells/well for each *Ncor2* shRNA and control shRNA. After 72h the cells were stimulated with CpG for 18h and then immune-profiling was performed using flow cytometry. We gated the live cells and first excluded macrophages using the F4/80 marker. Further we excluded plasmacytoid DCs and cDC2 by gating $CD11c^+$ $SiglecH^-$ and $CD24^+$ $CD11b^-$ respectively. Further all costimulatory and antigen markers were checked in $CD24^+$ cDC1. For intra cellular cytokine analysis we checked for IL-6, IL-12p0, IL-23p19, and IL-10 percent positive cells using MHC-II marker.

Co-culture of DCs with $CD4^+$ T-Cells and $CD8^+$ T-cells for assessing T-cell proliferation and differentiation

DC-T-cell co-culture experiments were performed according to well established protocol (53, 54). Naïve $CD4^+$ or $CD8^+$ T-cells were purified from spleen of TCR-transgenic OT-II or OT-I mice using $CD4^+$ or $CD8^+$ T-cell isolation kit. SMRT KD and control $CD8\alpha^+$ cDC1 DCs were seeded at a density of 10,000 cells/well in round bottom 96 well plates followed by pulsing with OVA peptide (323-339)/OT-II at 200nM concentration or OVA peptide (257–264)/OT-I was used at 5nM overnight. Further DCs were stimulated with CpG or pIC for 2h. After 2h, purified OT-II or OT-I T-cells were added at the density of 100,000 cells/well (1:10 ratio). Then T-cell proliferation and differentiation into distinct Th subtypes Th1, Th2, Th17 and Tregs, in case of OT-II, and cytotoxic T-cells, in case of OT-I, were analyzed by FACS. Proliferation was measured using an amine based dye (eFluor 670). The rate of T-cell proliferation was inversely proportional to the median

fluorescence intensity (MFI) measured in FACS after 72h of co-culture. For Th and cytotoxic T-cell differentiation profiling after 96h, the co-cultured T-cells were re-stimulated with PMA (10 ng/mL) and ionomycin (500 ng/mL) and followed by Brefeldin-A (10μg/mL) treatment for 5h to block the IC cytokines from being secreted. After 5h, fluorochrome conjugated antibodies specific to different T-cell subtypes were used to profile T-cells into Th1 (T-bet and IFN-γ), Th2 (GATA3, IL-13), Tregs (CD25, FoxP3, IL-10) and Th17 (RORγT, IL-17) or cytotoxic T-cells (perforin, IFN-γ, Granzyme-B). For gating effector T-cells we used CD44 as a marker.

Ex vivo OT-I T-cell cytotoxicity assay

OT-I cytotoxic assay was performed by seeding B16F10 cells at a density of 10,000 cells/well in a flat bottom 96 well plate. In parallel, control and SMRT KD cDC1 were seeded at a density of 10,000 cells/well and divided into two groups. Control and SMRT KD DCs from the 1st group were pulsed with OVA peptide (257–264)/OT-I at a concentration of 5nM and B16F10 cell lysate overnight and the 2nd group were left un-pulsed. Both the groups were activated for 2h with CpG. DCs from these two groups were co-cultured with naïve CD8^{+} T-cells purified from the spleen of TCR-transgenic OT-I mice. After 72h of co-culture, the OT-1 T-cells were then added on B16F10 cells that were previously seeded. After another 24h of co-culture of OT-1 cells and B16F10, the T-cells were stimulated with PMA (10ng/ml) and ionomycin (500ng/ml) for 5h and washed off. The adherent B16F10 cells were subjected to MTT assay at a working concentration of 0.5mg/ml for 4h. After 4h DMSO was added for another 1h and the absorbance was read at 570 nm. The absorbance values of B16F10 co-cultured with OT-1 cells from control and SMRT KD of group 1 were normalized with that of group 2.

The percentage of cell survival of B16F10 cells were calculated based on the formula:

$$\%\ \text{cell survival} = [(\text{Sample-Background})/(\text{B16F10 control-Background})] \times 100$$

In B16F10 control group the cells were untreated and absorbance of empty wells were taken as background.

Chromatin immuno-precipitation for p-STAT3

The ChIP for p-STAT3 was performed according to the methods optimized previously by Raghav and Meyer's lab. For ChIP assays, 40 x 10^{6} CD8α^{+} cDC1 MutuDCs were seeded in 15 cm^{2} plates and prepared for four ChIP assays by 10 min cross-linking with 1% formaldehyde (sigma) at room temperature followed by quenching using 2.5 M glycine (sigma) for 10 min. The plates were placed on ice and the cells were scraped and collected in 50 ml conical tubes. The cells were then washed three times using cold 1x PBS at 2,000 rpm for 10 min at 4°C and the cell pellets were stored at −80°C. At the day of the ChIP experiment, the cells were thawed on ice followed by lysis using Farham lysis buffer (5 mM PIPES pH 8.0, 85mM KCl, 0.5% NP-40 supplemented with protease and phosphatase inhibitors (Roche)) made in miliQ. The supernatant was aspirated and the pellet was resuspended in RIPA buffer (1% NP-40, 0.5% sodium deoxycholate, 0.1% SDS supplemented with Roche protease and phosphatase inhibitor tablet just before use). The chromatin was fragmented using a Bioruptor (Diagenode) sonicator for 30 min using high amplitude and 30s ON & 30s OFF cycles to obtain 200-500 bp size fragments. A cooling unit was used to circulate the cold water during sonication to avoid de-crosslinking because of overheating. After sonication, chromatin length was checked in agarose gel. The fragmented chromatin was centrifuged at 10,000 rpm for 5 min and then clear supernatant was collected in 15 ml conical tubes. The DNA concentration of the chromatin was estimated using a Nano-Drop (Thermo) and the chromatin was diluted with a RIPA buffer to use 150 μg/ml of chromatin for each IP. M-280 sheep anti-rabbit IgG dynabeads 40ul/IP was taken in a 1.5ml MCT tube. 1ml RIPA buffer was added to the beads and placed on a magnetic stand. The MCTs were inverted five times and allowed to stand for 3 min. The beads were washed in the same way three times. After the third wash the beads were centrifuged shortly and the remaining RIPA buffer was aspirated. To the beads, 5μl of mouse monoclonal anti-p-STAT3 (CST) was added to immunoprecipitated the chromatin complex at 4°C for 8h on rocker shaker. After 8h incubation, the beads were again placed on a magnetic stand and washed with RIPA to get rid of the unbound antibody. Chromatin was added to the beads and placed on a rotating rocker at 4°C overnight. Next day the tubes containing chromatin, antibody, and beads were taken out, placed on a magnetic stand and supernatant was aspirated. The beads were washed five times with LiCL IP wash buffer (100mM Tris pH7.5, 500mM LiCl, 1% NP-40, 1% sodium deoxycholate in miliQ) and two times with TE buffer (10mM Tris pH7.5, 0.1mM EDTA pH8 in miliQ). After removing the wash buffer completely, protein-bound chromatin complexes were eluted from beads using an elution buffer (1% SDS, 0.1M NaHCO3 in milli-Q water). The chromatin was incubated at room temperature for 30 min in an elution buffer. A short spin was given and the MCT was again placed on a magnetic stand to collect the eluted chromatin. The eluted chromatin was then reverse crosslinked by incubating the eluted supernatant at 65°C overnight on a heat block after adding 8 μl of 5 M NaCl. Next day DNA was purified from the reverse cross-linked chromatin by proteinase-K and RNase digestion followed by purification using PCR purification kit (Qiagen). The purified DNA was eluted in 40μl of elution buffer.

Chromatin immuno-precipitation for SMRT

The ChIP for SMRT was performed according to the methods optimized previously by Raghav and Deplancke's lab (25, 55). In short, the cells were lysed in a nuclei extraction buffer for 10 min at 4°C while shaking to isolate the nuclei. The isolated nuclei were then washed using a protein extraction buffer at room temperature for 10 min. Washed nuclei were resuspended in chromatin extraction and incubated for 20 min on ice. The chromatin was fragmented using a Bioruptor (Diagenode) sonicator to obtain 200-500 bp-sized fragments. The fragmented chromatin was centrifuged at 17,000g for 10 min and then clear supernatant was collected in chilled 15ml falcon tubes. The DNA concentration of the chromatin was estimated using a NanoDrop and the sonicated chromatin was diluted with ChIP dilution buffer to get 100 µg/ml of chromatin for each IP. BSA and ssDNA (Salmon Sperm DNA) -preblocked protein-A sepharose (80 µl/IP) beads were added to the samples and incubated for 2h to remove non-specific- binding chromatin. To the supernatant, 5 µl/IP rabbit polyclonal anti-SMRT antibody (Abcam) was added to immuno-precipitate the chromatin complex at 4°C overnight. After the overnight incubation, 50µl blocked beads were added to each sample and incubated for 90 min at 4°C to pull down the respective antibody-chromatin complexes. The beads were then washed four times with a low salt wash buffer followed by two washes with high salt wash buffer, lithium chloride wash buffer and tris-EDTA (TE) buffer. After removing the wash buffer completely, protein-bound chromatin complexes were eluted from beads for 30 min using an elution buffer. The eluted chromatin was then reverse-crosslinked by incubating the eluted supernatant at 65°C overnight on a heat block after adding 8µl of 5M NaCl. The next day, DNA was purified from the reverse crosslinked chromatin by proteinase and RNase digestion followed by purification using Qiagen DNA purification columns. The purified DNA was eluted in 50µl of Qiagen elution buffer.

ChIP/RNA-seq library preparation for sequencing

For RNA-seq library preparation 2ug of total RNA was used to isolate mRNA using magnetic beads with mRNA isolation kit (PolyA mRNA isolation module, NEB). Later mRNA library preparation kit, NEB, was used for RNA-seq library preparation according to manufacturer's protocol. Concentration of the libraries were estimated by Qubit 2.0 (Invitrogen) and fragment sizes were analyzed in Bio-analyzer (Agilent). The libraries were then sequenced on Illumina NextSeq 550 platform.

Similarly for ChIP seq 30 µl ChIP-DNA was processed for library preparation according to ChIP-seq library preparation protocol (NEB) (25). After library preparation and quality check, the libraries were sent to NGS service provider (Sci Genome, Bangalore, India) for Illumina sequencing using NextSeq-550 instrument.

Western blotting

Cells were collected in RIPA buffer (0.5 M EDTA, 1 M Tris-Cl pH7.5, 1 M NaCl, 200 mM, Roche protease inhibitor) at 0h, 2h and 6h CpG stimulation. Cells were lysed completely by sonication of the samples in Bioruptor (Diagenode) for 10 min using high amplitude and 30s ON & 30s OFF cycles. Protein concentrations were measured in 96 well plates using BCA protein assay kit (BioRad) at 562nM. For western blot of phospho and its respective total protein molecule we first probed the membrane with phospho-antibodies, stripped and re-probed the same membrane with respective total antibodies. For densitometric analysis we first normalized phosphorylated form of STAT3/mTOR with their respective loading controls. The similar approach was followed for its corresponding total protein. Finally, the ratio of normalized values were plotted as relative intensity.

Delayed type hypersensitivity assay

DTH was performed using culture grade ovalbumin (OVA) from chicken egg (Sigma) dissolved in 1x PBS at a concentration of 1mg/ml and filtered through 0.2-micron PES syringe filter. 1.5ml alum and 1.5ml OVA was added in a glass beaker and passed through a glass syringe multiple times to make an emulsion. 300µl per mice was injected subcutaneously in the back behind ears in each mice for OVA immunization. After 14 days control and SMRT KD DCs were pulsed with OVA (100ug/ml) for 4 h. Cells were then stimulated with CpG. After 2h of stimulation the cells were dissociated and injected at 10 x 10^6 cells/mice. Further after 7 days OVA (20mg/ml) was heated at 80°C for 2h, cooled, and injected in foot pad of mice (25µl/mice). 1x PBS was injected in the alternative footpad. Paw thickness was measured till 72h using Vernier caliper. After 72h the popliteal and inguinal lymph nodes were isolated and checked for T-bet IFN-γ as well as RORγt IL-17. Paw swelling was plotted at different time points and two-way ANOVA with Tukey's test was performed between different mice groups.

Tumor cell lysate preparation

Tumor lysate was prepared from previous reports with some modifications (56). B16/F10 tumor cells were adjusted to 3×10^6 cells/ml in DMEM medium. Cells were subjected to three freeze (– 80°C)/thaw (40°C) cycles of minimum 20 min each. The lysed cells were checked under trypan blue staining and centrifuged at

12,000rpm for 15 min. The supernatant was passed through a 40μm cell strainer before adding to cDC1 seeded at a density of 3 x 106 (DC: tumor cell ratio of 1:1).

B16F10 tumor model

0.5 x 10^6 Control and SMRT KD cDC1 cells were pulsed with B16F10 cell lysate at 1:1 (DCs:B16F10) ratio overnight followed by CpG challenge for 2h. These cells were then injected in the left flank of mice subcutaneously (s.c) and a booster dose of pulsed and CpG challenged cDC1 was re-injected 3 days later. 7 days after booster dose, 0.1 x 10^6 B16F10 cells were injected subcutaneously in the right flank of the same mice. Tumor growth was measured every day using a vernier caliper till 16 days. Tumor volume was plotted at different days and two-way ANOVA with Tukey's test was performed between different mice groups. Further, tumors were removed, weighed, and dissociated to make single cell suspensions.

Isolation of tumor and tumor re-stimulation

For IC perforin, granzyme-B, and IFN-γ staining, single cell suspensions were *ex vivo* re-stimulated with 10ng/ml PMA, 500ng/ml ionomycin, and 5 μg/mL Brefeldin A for 5h. Cells were labelled with indicated surface-staining antibodies, fixed with 2% PFA, permeabilized with permeabilization buffer and stained with IC antibodies.

RNA-seq data processing and analysis

Raw reads of SMRT KD RNA-seq samples and its matched control in unstimulated and 6h CpG stimulation were checked for quality using FASTQC (57), and aligned to mouse genome (UCSC mm10) using hisat2 (58) (with default parameter). Similarly, raw reads of NCoR1 KD and its matched control RNA-seq were processed for quality control and alignment. Raw counts of genes were extracted using featureCount (featureCounts -p -B) (59). Principal component analysis was performed on variance stabilized transformed (vst) values from DESeq2 (60) using the plotPCA function and plotted using ggplot2 (61). Further, differential gene expression analysis was performed between NCoR1/SMRT KD compared to its matched control in unstimulated and 6h CpG stimulation condition. Genes were filtered based on log2foldchange (upregulated >= 1 and downregulated<= -1) and adjusted P-value (< 0.05). Total differentially expressed genes were combined from all the comparisons and unsupervised k-means clustering were performed based on log2foldchange values and divided into six clusters. Pathway enrichment analysis for each cluster was performed using Ingenuity pathway analysis.

ChIP-seq data processing and analysis

SMRT ChIP-seq raw reads in unstimulated and 6h CpG stimulation were checked for quality using FASTQC and aligned to mouse genome (RefSeq mm10) using bowtie2 (62). Reads were filtered using MarkDuplicates function of Picard and mapping quality >=10 using SAMtools (63, 64). Peak calling was performed using findPeaks (Homer) and factor as style. Peak calling for NCoR1 ChIP-seq data from our previous study were performed with reads down sampled to the level of SMRT i.e. 9M. Distribution analysis of peaks based on distance relative to TSS were performed using ChIPSeeker (65). Peaks from both NCoR1 and SMRT were merged using bedops merge command and consensus peaks were generated for further downstream analysis (66) GeneOverlap R package were used to identify differentially expressed genes that are the direct target of SMRT (67).

ChIP-seq peak analysis

Differential binding analysis for NCoR1 and SMRT were carried out on the merged peak using the getDifferentialPeaks program of Homer with cut-off of 2-fold enrichment over background (68). Peaks were filtered out that didn't show any differential binding in any of the comparisons. Differential peaks were then categorized based on fold change. Peaks from different categories were annotated to nearest genes using the ChIPseeker R package (69). *De novo* motif enrichment analysis was performed using findMotifs.pl (size -50, 50 -len 8, 10, 12) using background generated from provided input genomic regions. P-value<=1e-10 were used to filter significantly enriched TF motifs. KEGG pathway enrichment analysis of differentially expressed genes associated with each binding category were performed using clusterProfiler R package (69).

Data availability statement

The datasets presented in this study can be found in online repositories. The names of the repository/repositories and accession number(s) can be found below: https://www.ebi.ac.uk/arrayexpress/, E-MTAB-10070; https://www.ebi.ac.uk/

arrayexpress/, E-MTAB-10069; https://www.ebi.ac.uk/arrayexpress/, E-MTAB-10864.

Ethics statement

The studies involving human participants were reviewed and approved by Institutional Ethics Committee, Kalinga Institute of Industrial Technology (KIIT) University. The patients/participants provided their written informed consent to participate in this study. The animal study was reviewed and approved by Institutional Animal Ethics Committee-Institute of Life Sciences.

Author contributions

AJ, AA, GPM, BG, HAO, SBS, and SR conceptualized the study, AJ, AA, KS, SS, AT, VKB, and APM were involved in performing experiments and interpretation of the results. GPM and SR did all the computational analysis of the genomics data. AJ, AA, GPM, and SR wrote the manuscript. Funding for the study was secured by SR from different funding agencies acknowledged in funding section. All authors contributed to the article and approved the submitted version.

Funding

This study is supported by grants from SERB (EMR/2016/000717, CRG/2019/005893), DST-SNSF (DST/INT/SWISS/SNSF/P-47/2015), DBT Ramalingaswami fellowship, DBT (BT/PR15908/MED/12/725/2016). ILS provided intramural support and infrastructure.

Acknowledgments

We are sincerely thankful to HAO for providing us the DC cell lines, OT-I, OT-II, and FLT-3 transgenic mice. We would like to thank ILS sequencing and High performance computing facility. We would like to thank Subhasish Prusty for helping in western experiments and Niyati Das for helping in animal experiments. AJ is supported by ILS fellowship, AA is supported by DBT-SRF, GPM is supported by DBT BINC fellowship, KS is supported by UGC-SRF, SS is supported by ILS fellowship, APM is supported by CSIR funding, VKB is supported by ILS tribal flagship fellowship, AT is supported by DST INSPIRE.

Conflict of interest

The authors declare that the research was conducted in the absence of any commercial or financial relationships that could be construed as a potential conflict of interest.

Publisher's note

Supplementary material

The Supplementary Material for this article can be found online at: https://www.frontiersin.org/articles/10.3389/fimmu.2022.910705/full#supplementary-material

SUPPLEMENTARY FILE 1
Excel file having list of differentially expressed genes (DEGs) in SMRT KD compared to control at 0h and 6h CpG stimulation.

SUPPLEMENTARY FILE 2
Excel file having a list of annotations of direct target genes that are bound and differentially expressed upon SMRT KD at 0h and 6h CpG stimulation.

SUPPLEMENTARY FILE 3
Excel file having list of enriched Ingenuity pathway terms for direct target genes of SMRT that upregulated and downregulated in SMRT KD compared to control at 6h CpG stimulation.

SUPPLEMENTARY FILE 4
Excel file having list of DEGs divided in 6 k-means clusters based on Log2 fold change in NCoR1 KD and SMRT KD compared to Control DCs in Uns and 6h CpG stimulated condition

SUPPLEMENTARY FILE 5
Excel file having list of enriched IPA pathway terms for all the 6 k-means clusters.

SUPPLEMENTARY FILE 6
Excel file having list of enriched KEGG terms for list of direct target genes of differential binding sites of NCoR1 and SMRT.

References

1. Steinman RM. Dendritic cells: understanding immunogenicity. *Eur J Immunol* (2007) 37 Suppl 1:S53–60. doi: 10.1002/eji.200737400

2. Steinman RM, Hawiger D, Nussenzweig MC. Tolerogenic dendritic cells. *Annu Rev Immunol* (2003) 21:685–711. doi: 10.1146/annurev.immunol.21.120601.141040

3. Hilligan KL, Ronchese F. Antigen presentation by dendritic cells and their instruction of CD4+ T helper cell responses. *Cell Mol Immunol* (2020) 17(6):587–99. doi: 10.1038/s41423-020-0465-0

4. Manicassamy S, Pulendran B. Dendritic cell control of tolerogenic responses. *Immunol Rev* (2011) 241(1):206–27. doi: 10.1111/j.1600-065X.2011.01015.x

5. Abou Fakher FH, Rachinel N, Klimczak M, Louis J, Doyen N. TLR9-dependent activation of dendritic cells by DNA from leishmania major favors Th1 cell development and the resolution of lesions. *J Immunol* (2009) 182(3):1386–96. doi: 10.4049/jimmunol.182.3.1386

6. Schnorrer P, Behrens GMN, Wilson NS, Pooley JL, Smith CM, El-Sukkari D, et al. The dominant role of CD8+ dendritic cells in cross-presentation is not dictated by antigen capture. *Proc Natl Acad Sci U.S.A.* (2006) 103(28):10729–34. doi: 10.1073/pnas.0601956103

7. Musumeci A, Lutz K, Winheim E, Krug AB. What makes a pDC: Recent advances in understanding plasmacytoid DC development and heterogeneity. *Front Immunol* (2019) 10:1222. doi: 10.3389/fimmu.2019.01222

8. Wculek SK, Cueto FJ, Mujal AM, Melero I, Krummel MF, Sancho D. Dendritic cells in cancer immunology and immunotherapy. *Nat Rev Immunol* (2020) 20(1):7–24. doi: 10.1038/s41577-019-0210-z

9. Kawasaki T, Kawai T. Toll-like receptor signaling pathways. *Front Immunol* (2014) 5:461. doi: 10.3389/fimmu.2014.00461

10. Della Mina E, Borghesi A, Zhou H, Bougarn S, Boughorbel S, Israel L, et al. Inherited human IRAK-1 deficiency selectively impairs TLR signaling in fibroblasts. *Proc Natl Acad Sci U.S.A.* (2017) 114(4):E514–23. doi: 10.1073/pnas.1620139114

11. Kawai T, Akira S. Signaling to NF-kappaB by toll-like receptors. *Trends Mol Med* (2007) 13(11):460–9. doi: 10.1016/j.molmed.2007.09.002

12. Kimura A, Naka T, Muta T, Takeuchi O, Akira S, Kawase I, et al. Suppressor of cytokine signaling-1 selectively inhibits LPS-induced IL-6 production by regulating JAK-STAT. *Proc Natl Acad Sci U.S.A.* (2005) 102(47):17089–94. doi: 10.1073/pnas.0508517102

13. Liu BS, Cao Y, Huizinga TW, Hafler DA, Toes REM. TLR-mediated STAT3 and ERK activation controls IL-10 secretion by human b cells. *Eur J Immunol* (2014) 44(7):2121–9. doi: 10.1002/eji.201344341

14. Melillo JA, Song L, Bhagat G, Blazquez AB, Plumlee CR, Lee C, et al. Dendritic cell (DC)-specific targeting reveals Stat3 as a negative regulator of DC function. *J Immunol* (2010) 184(5):2638–45. doi: 10.4049/jimmunol.0902960

15. Maldonado RA, von Andrian UH. How tolerogenic dendritic cells induce regulatory T cells. *Adv Immunol* (2010) 108:111–65. doi: 10.1016/B978-0-12-380995-7.00004-5

16. Sallusto F, Lanzavecchia A. The instructive role of dendritic cells on T-cell responses. *Arthritis Res* (2002) 4 Suppl 3:S127–32. doi: 10.1186/ar567

17. Mosser DM, Zhang X. Interleukin-10: new perspectives on an old cytokine. *Immunol Rev* (2008) 226:205–18. doi: 10.1111/j.1600-065X.2008.00706.x

18. Nencioni A, Grunebach F, Zobywlaski A, Denzlinger C, Brugger W, Brossart P. Dendritic cell immunogenicity is regulated by peroxisome proliferator-activated receptor gamma. *J Immunol* (2002) 169(3):1228–35. doi: 10.4049/jimmunol.169.3.1228

19. Tel-Karthaus N, Kers-Rebel ED, Looman MW, Ichinose H, de Vries CJ, Ansems M. Nuclear receptor Nur77 deficiency alters dendritic cell function. *Front Immunol* (2018) 9:1797. doi: 10.3389/fimmu.2018.01797

20. Heming M, Gran S, Jauch SL, Fischer-Riepe L, Russo A, Klotz L, et al. Peroxisome proliferator-activated receptor-gamma modulates the response of macrophages to lipopolysaccharide and glucocorticoids. *Front Immunol* (2018) 9:893. doi: 10.3389/fimmu.2018.00893

21. Sohn YC, Kwak E, Na Y, Lee JW, Lee SK. Silencing mediator of retinoid and thyroid hormone receptors and activating signal cointegrator-2 as transcriptional coregulators of the orphan nuclear receptor Nur77. *J Biol Chem* (2001) 276 (47):43734–9. doi: 10.1074/jbc.M107208200

22. Jepsen K, Rosenfeld MG. Biological roles and mechanistic actions of co-repressor complexes. *J Cell Sci* (2002) 115(Pt 4):689–98. doi: 10.1242/jcs.115.4.689

23. Ghisletti S, Huang W, Jepsen K, Benner C, Hardiman G, Rosenfeld MG, et al. Cooperative NCoR/SMRT interactions establish a corepressor-based strategy for integration of inflammatory and anti-inflammatory signaling pathways. *Genes Dev* (2009) 23(6):681–93. doi: 10.1101/gad.1773109

24. Sander J, Schmidt SV, Cirovic B, McGovern N, Papantonopoulou O, Hardt A-L, et al. Cellular differentiation of human monocytes is regulated by time-dependent interleukin-4 signaling and the transcriptional regulator NCOR2. *Immunity* (2017) 47(6):1051–1066 e12. doi: 10.1016/j.immuni.2017.11.024

25. Ahad A, Stevanin M, Smita S, Mishra GP, Gupta D, Waszak S, et al. NCoR1: Putting the brakes on the dendritic cell immune tolerance. *iScience* (2019) 19:996–1011. doi: 10.1016/j.isci.2019.08.024

26. Fuertes Marraco SA, Grosjean F, Duval A, Rosa M, Lavanchy C, Ashok D, et al. Novel murine dendritic cell lines: a powerful auxiliary tool for dendritic cell research. *Front Immunol* (2012) 3:331. doi: 10.3389/fimmu.2012.00331

27. Nish SA, Schenten D, Wunderlich FT, Pope SD, Gao Y, Hoshi N, et al. T Cell-intrinsic role of IL-6 signaling in primary and memory responses. *Elife* (2014) 3:e01949. doi: 10.7554/eLife.01949

28. Maloy KJ, Kullberg MC. IL-23 and Th17 cytokines in intestinal homeostasis. *Mucosal Immunol* (2008) 1(5):339–49. doi: 10.1038/mi.2008.28

29. Alzabin S, Williams RO. Effector T cells in rheumatoid arthritis: lessons from animal models. *FEBS Lett* (2011) 585(23):3649–59. doi: 10.1016/j.febslet.2011.04.034

30. Hemdan NY, Birkenmeier G, Wichmann G, Abu El-Saad AM, Krieger T, Conrad K, et al. Interleukin-17-producing T helper cells in autoimmunity. *Autoimmun Rev* (2010) 9(11):785–92. doi: 10.1016/j.autrev.2010.07.003

31. Utku N, Boerner A, Tomschegg A, Bennai-Sanfourche F, Bulwin G-C, Heinemann T, et al. TIRC7 deficiency causes in vitro and in vivo augmentation of T and b cell activation and cytokine response. *J Immunol* (2004) 173(4):2342–52. doi: 10.4049/jimmunol.173.4.2342

32. Kalinski P, Urban J, Narang R, Berk E, Wieckowski E, Muthuswamy R. Dendritic cell-based therapeutic cancer vaccines: what we have and what we need. *Future Oncol* (2009) 5(3):379–90. doi: 10.2217/fon.09.6

33. Liu X, Zhang P, Bao Y, Han Y, Wang Y, Zhang Q, et al. Zinc finger protein ZBTB20 promotes toll-like receptor-triggered innate immune responses by repressing IkappaBalpha gene transcription. *Proc Natl Acad Sci U.S.A.* (2013) 110(27):11097–102. doi: 10.1073/pnas.1301257110

34. Zhou S, Cerny AM, Fitzgerald KA, Kurt-Jones EA, Finberg RW. Role of interferon regulatory factor 7 in T cell responses during acute lymphocytic choriomeningitis virus infection. *J Virol* (2012) 86(20):11254–65. doi: 10.1128/JVI.00576-12

35. Suryawanshi A, Manoharan I, Hong Y, Swafford D, Majumdar T, Taketo MM, et al. Canonical wnt signaling in dendritic cells regulates Th1/Th17 responses and suppresses autoimmune neuroinflammation. *J Immunol* (2015) 194(7):3295–304. doi: 10.4049/jimmunol.1402691

36. Uto T, Fukaya T, Takagi H, Arimura K, Nakamura T, Kojima N, et al. Clec4A4 is a regulatory receptor for dendritic cells that impairs inflammation and T-cell immunity. *Nat Commun* (2016) 7:11273. doi: 10.1038/ncomms11273

37. Chang J, Kunkel SL, Chang CH. Negative regulation of MyD88-dependent signaling by IL-10 in dendritic cells. *Proc Natl Acad Sci U.S.A.* (2009) 106 (43):18327–32. doi: 10.1073/pnas.0905815106

38. Hedrich CM, Rauen T, Apostolidis SA, Grammatikos AP, Rodriguez Rodriguez N, Ioannidis C, et al. Stat3 promotes IL-10 expression in lupus T cells through trans-activation and chromatin remodeling. *Proc Natl Acad Sci U.S.A.* (2014) 111(37):13457–62. doi: 10.1073/pnas.1408023111

39. Garber M, Yosef N, Goren A, Raychowdhury R, Thielke A, Guttman M, et al. A high-throughput chromatin immunoprecipitation approach reveals principles of dynamic gene regulation in mammals. *Mol Cell* (2012) 47(5):810–22. doi: 10.1016/j.molcel.2012.07.030

40. Wu L. A Flt3L encounter: mTOR signaling in dendritic cells. *Immunity* (2010) 33(4):580–2. doi: 10.1016/j.immuni.2010.10.001

41. Thomson AW, Turnquist HR, Raimondi G. Immunoregulatory functions of mTOR inhibition. *Nat Rev Immunol* (2009) 9(5):324–37. doi: 10.1038/nri2546

42. Li P, Spann NJ, Kaikkonen MU, Lu M, Oh DY, Fox JN, et al. NCoR repression of LXRs restricts macrophage biosynthesis of insulin-sensitizing omega 3 fatty acids. *Cell* (2013) 155(1):200–14. doi: 10.1016/j.cell.2013.08.054

43. Fan R, Toubal A, Goñi S, Drareni K, Huang Z, Alzaid F, et al. Loss of the co-repressor GPS2 sensitizes macrophage activation upon metabolic stress induced by obesity and type 2 diabetes. *Nat Med* (2016) 22(7):780–91. doi: 10.1038/nm.4114

44. Iyer SS, Cheng G. Role of interleukin 10 transcriptional regulation in inflammation and autoimmune disease. *Crit Rev Immunol* (2012) 32(1):23–63. doi: 10.1615/CritRevImmunol.v32.i1.30

45. Samarasinghe R, Tailor P, Tamura T, Kaisho T, Akira S, Ozato K. Induction of an anti-inflammatory cytokine, IL-10, in dendritic cells after toll-like receptor signaling. *J Interferon Cytokine Res* (2006) 26(12):893–900. doi: 10.1089/jir.2006.26.893

46. Brightbill HD, Plevy SE, Modlin RL, Smale ST. A prominent role for Sp1 during lipopolysaccharide-mediated induction of the IL-10 promoter in macrophages. *J Immunol* (2000) 164(4):1940–51. doi: 10.4049/jimmunol.164.4.1940

47. Haidinger M, Poglitsch M, Geyeregger R, Kasturi S, Zeyda M, Zlabinger GJ, et al. A versatile role of mammalian target of rapamycin in human dendritic cell function and differentiation. *J Immunol* (2010) 185(7):3919–31. doi: 10.4049/jimmunol.1000296

48. Chen Z, Laurence A, Kanno Y, Pacher-Zavisin M, Zhu BM, Tato C, et al. Selective regulatory function of Socs3 in the formation of IL-17-secreting T cells. *Proc Natl Acad Sci U.S.A.* (2006) 103(21):8137–42. doi: 10.1073/pnas.0600666103

49. Rigby RJ, Simmons JG, Greenhalgh CJ, Alexander WS, Lund PK. Suppressor of cytokine signaling 3 (SOCS3) limits damage-induced crypt hyper-proliferation and inflammation-associated tumorigenesis in the colon. *Oncogene* (2007) 26 (33):4833–41. doi: 10.1038/sj.onc.1210286

50. Lee SO, Andey T, Jin UH, Kim K, Singh M, Safe S. The nuclear receptor TR3 regulates mTORC1 signaling in lung cancer cells expressing wild-type p53. *Oncogene* (2012) 31(27):3265–76. doi: 10.1038/onc.2011.504

51. Ohta A, Sato N, Yahata T, Ohmi Y, Santa K, Sato T, et al. Manipulation of Th1/Th2 balance in vivo by adoptive transfer of antigen-specific Th1 or Th2 cells. *J Immunol Methods* (1997) 209(1):85–92. doi: 10.1016/S0022-1759(97)00152-X

52. Li S, Yin H, Zhang K, Wang T, Yang Y, Liu X, et al. Effector T helper cell populations are elevated in the bone marrow of rheumatoid arthritis patients and correlate with disease severity. *Sci Rep* (2017) 7(1):4776. doi: 10.1038/s41598-017-05014-8

53. Smita S, Ahad A, Ghosh A, Biswas VK, Koga MM, Gupta B, et al. Importance of EMT factor ZEB1 in cDC1 "MutuDC line" mediated induction of Th1 immune response. *Front Immunol* (2018) 9:2604. doi: 10.3389/fimmu.2018.02604

54. Smita S, Ghosh A, Biswas VK, Ahad A, Podder S, Jha A, et al. Zbtb10 transcription factor is crucial for murine cDC1 activation and cytokine secretion. *Eur J Immunol* (2021) 51(5):1126–42. doi: 10.1002/eji.202048933

55. Raghav SK, Waszak SM, Krier I, Gubelmann C, Isakova A, Mikkelsen TS, et al. Integrative genomics identifies the corepressor SMRT as a gatekeeper of adipogenesis through the transcription factors C/EBPbeta and KAISO. *Mol Cell* (2012) 46(3):335–50. doi: 10.1016/j.molcel.2012.03.017

56. Rainone V, Martelli C, Ottobrini L, Biasin M, Texido G, Degrassi A, et al. Immunological characterization of whole tumour lysate-loaded dendritic cells for cancer immunotherapy. *PloS One* (2016) 11(1):e0146622. doi: 10.1371/journal.pone.0146622

57. Andrews S, Krueger, Felix, Segonds-Pichon. *FastQC: A quality control tool for high throughput sequence data*. (2012). Available at: https://www.bioinformatics.babraham.ac.uk/projects/fastqc/

58. Kim D, Paggi JM, Park C, Bennett C, Salzberg SL. Graph-based genome alignment and genotyping with HISAT2 and HISAT-genotype. *Nat Biotechnol* (2019) 37(8):907–15. doi: 10.1038/s41587-019-0201-4

59. Liao Y, Smyth GK, Shi W. featureCounts: an efficient general purpose program for assigning sequence reads to genomic features. *Bioinformatics* (2014) 30(7):923–30. doi: 10.1093/bioinformatics/btt656

60. Love MI, Huber W, Anders S. Moderated estimation of fold change and dispersion for RNA-seq data with DESeq2. *Genome Biol* (2014) 15(12):550. doi: 10.1186/s13059-014-0550-8

61. Wickham H. *ggplot2: Elegant graphics for data analysis*. (2016). Springer-Verlag New York. Available at: https://ggplot2.tidyverse.org.

62. Langmead B, Salzberg SL. Fast gapped-read alignment with bowtie 2. *Nat Methods* (2012) 9(4):357–9. doi: 10.1038/nmeth.1923

63. Li H, Handsaker B, Wysoker A, Fennell T, Ruan J, Homer N, et al. The sequence Alignment/Map format and SAMtools. *Bioinformatics* (2009) 25 (16):2078–9. doi: 10.1093/bioinformatics/btp352

64. *Picard toolkit*. Broad Institute (2019). Available at: https://broadinstitute.github.io/picard/

65. Yu G, Wang LG, He QY. ChIPseeker: an R/Bioconductor package for ChIP peak annotation, comparison and visualization. *Bioinformatics* (2015) 31 (14):2382–3. doi: 10.1093/bioinformatics/btv145

66. Neph S, Kuehn MS, Reynolds AP, Haugen E, Thurman RE, Johnson AK, et al. BEDOPS: high-performance genomic feature operations. *Bioinformatics* (2012) 28(14):1919–20. doi: 10.1093/bioinformatics/bts277

67. Li Shen MS. *GeneOverlap: Test and visualize gene overlaps*. (2022). R package version 1.32.0. Available at: http://shenlab-sinai.github.io/shenlab-sinai/.

68. Heinz S, Benner C, Spann N, Bertolino E, Lin YC, Laslo P, et al. Simple combinations of lineage-determining transcription factors prime cis-regulatory elements required for macrophage and b cell identities. *Mol Cell* (2010) 38(4):576–89. doi: 10.1016/j.molcel.2010.05.004

69. Yu G, Wang LG, Han Y, He QY. clusterProfiler: an r package for comparing biological themes among gene clusters. *OMICS* (2012) 16(5):284–7. doi: 10.1089/omi.2011.0118